JOURNAL OF PETROLOGY | VOLUME 47 | NUMBER 10 | PAGES 1973–1996 | 2006 | doi:10.1093/petrology/egl033

Temperature and Bulk Composition Control on the Growth of Monazite and Zircon During Low-pressure Anatexis (Mount Stafford, Central Australia)

DANIELA RUBATTO[1]*, JÖRG HERMANN[1] AND IAN S. BUICK[2]

[1]RESEARCH SCHOOL OF EARTH SCIENCES, THE AUSTRALIAN NATIONAL UNIVERSITY, CANBERRA 0200 ACT, AUSTRALIA

[2]SCHOOL OF GEOSCIENCES, MONASH UNIVERSITY, MELBOURNE 3800 VIC., AUSTRALIA

RECEIVED OCTOBER 4, 2005; ACCEPTED MAY 15, 2006; ADVANCE ACCESS PUBLICATION JUNE 17, 2006

The formation, age and trace element composition of zircon and monazite were investigated across the prograde, low-pressure metamorphic sequence at Mount Stafford (central Australia). Three pairs of inter-layered metapelites and metapsammites were sampled in migmatites from amphibolite-facies ($T \sim 600^\circ C$) to granulite-facies conditions ($T \sim 800^\circ C$). Sensitive high-resolution ion microprobe U–Pb dating on metamorphic zircon rims and on monazite indicates that granulite-facies metamorphism occurred between ~1795 and 1805 Ma. The intrusion of an associated granite was coeval with metamorphism at 1802 ± 3 Ma and is unlikely to be the heat source for the prograde metamorphism. Metamorphic growth of zircon started at $T \sim 750^\circ C$, well above the pelite solidus. Zircon is more abundant in the metapelites, which experienced higher degrees of partial melting compared with the associated metapsammites. In contrast, monazite growth initiated under sub-solidus prograde conditions. At granulite-facies conditions two distinct metamorphic domains were observed in monazite. Textural observations, petrology and the trace element composition of monazite and garnet provide evidence that the first metamorphic monazite domain grew prior to garnet during prograde conditions and the second in equilibrium with garnet and zircon close to the metamorphic peak. Ages from sub-solidus, prograde and peak metamorphic monazite and zircon are not distinguishable within error, indicating that heating took place in less than 20 Myr.

KEY WORDS: *accessory phases; anatexis; trace element partitioning; U–Pb dating*

INTRODUCTION

The geochronology of amphibolite- to granulite-facies rocks is commonly dependent on the U–Pb dating of zircon and monazite. Thus the understanding of the behaviour of these two accessory minerals during medium- to high-temperature metamorphism is crucial for age interpretation. The processes by which zircon and monazite (re)crystallize (as a result of melting reactions or melt crystallization, solid-state metamorphic reactions or fluid infiltration), the conditions in which they form, the events that they record, and how the *P–T* conditions of their formation can be established have recently been under intense scrutiny. Significant work has focused on characterizing the appearance (zoning patterns, textures and inclusion assemblages) and trace element composition of metamorphic zircon (Williams & Claesson, 1987; Heaman *et al.*, 1990; Hinton & Upton, 1991; Williams *et al.*, 1996; Williams, 2001; Rubatto, 2002; Corfu *et al.*, 2003; Hoskin & Schaltegger, 2003) and on the processes leading to its formation (Fraser *et al.*, 1997; Roberts & Finger, 1997; Degeling *et al.*, 2001; Williams, 2001). The way that monazite is affected by metamorphism has also been extensively investigated (e.g. Rubatto *et al.*, 2001; Williams, 2001; Wing *et al.*, 2003; Fitzsimons *et al.*, 2005): monazite will first form at lower metamorphic grade (lower to mid-amphibolite-facies conditions) than zircon and may lose its Pb memory as a result of solid-state resorption or re-precipitation reactions earlier during prograde metamorphism. In

*Corresponding author. Telephone: ++61 2 61255157. Fax: ++61 2 61258345. E-mail: Daniela.Rubatto@anu.edu.au

contrast, zircon generally, but not always (Degeling *et al.*, 2001), forms in the presence of melt and once formed retains its isotopic memory up to extremely high temperatures (Vavra *et al.*, 1996; Oliver *et al.*, 1999; Rubatto *et al.*, 2001; Williams, 2001).

Most recently, the focus has shifted toward the petrology of zircon and monazite, their equilibrium with major rock-forming metamorphic minerals and their trace element compositions (e.g. Pyle & Spear, 1999; Degeling *et al.*, 2001; Foster *et al.*, 2002; Rubatto, 2002; Hermann & Rubatto, 2003; Hoskin & Schaltegger, 2003; Whitehouse & Platt, 2003; Wing *et al.*, 2003; Hokada & Harley, 2004; Kelly & Harley, 2005; Watson & Harrison, 2005; Buick *et al.*, 2006). Trace elements have been used for zircon thermometry (Watson & Harrison, 2005) and for assessing equilibrium between zircon and monazite and other minerals (Foster *et al.*, 2002; Rubatto, 2002; Hermann & Rubatto, 2003; Whitehouse & Platt, 2003; Hokada & Harley, 2004; Kelly & Harley, 2005; Buick *et al.*, 2006).

From the large number of studies of metamorphic U–Pb minerals it also appears that there might be a difference in metamorphic behaviour of zircon and monazite according to host-rock composition; for example, the formation of monazite in metasediments depends on the Ca and/or Al content of the rock (Wing *et al.*, 2003; Fitzsimons *et al.*, 2005). Differences are also found in the distribution of trace elements between zircon and garnet at different temperatures (see Rubatto *et al.*, 2001; Hokada & Harley, 2004).

We address the issue of the response of zircon and monazite to prograde metamorphism and partial melting using petrography, sensitive high-resolution ion microprobe (SHRIMP) U–Pb dating and trace element analysis for a representative suite of rocks from Mount Stafford (central Australia). Mount Stafford is host to a well-studied Palaeoproterozoic low-pressure metamorphic sequence from greenschist to granulite facies, which reached melting conditions below 4 kbar, partly in the andalusite field (Greenfield *et al.*, 1998; White *et al.*, 2003). The detailed work of White *et al.* (2003) provides temperature estimates, as well as melting reactions and calculated melt proportions in different rock types (pelitic and psammitic protoliths, respectively). This provides an excellent basis to study the behaviour of zircon and monazite as a function of temperature, bulk-rock composition and degree of partial melting in rocks. We address these issues using zircon and monazite petrography, SHRIMP U–Pb ages and trace element contents for a representative suite of rocks.

REGIONAL SETTING AND METAMORPHISM

Mount Stafford is located ~170 km NW of Alice Springs in central Australia. It constitutes the NW end of the Anmatjira–Reynolds Range area, within the Proterozoic Arunta Inlier (Fig. 1a). The Mount Stafford area is dominated by metamorphosed pelitic to psammitic sediments (Mount Stafford Beds) and large deformed granitoids (Mount Stafford granite). The majority of the area studied consists of aluminous metapelites, interbedded with metapsammite layers on a centimetre to metre scale (Vernon *et al.*, 1990; Greenfield *et al.*, 1998; White *et al.*, 2003). Rare metamorphosed diorite sills cross-cut the sedimentary sequence. According to Collins *et al.* (1991), the Mont Stafford metasediments and the intruding diorite sills underwent three phases of deformation ascribed to the main tectonic cycle. Deformation mainly translated into folding from tight, metre-scale folds to open, isoclinal and kilometre-scale folds. Opposite to folding, foliation and lineation are generally weak and localized.

The metamorphic conditions at Mount Stafford increase from greenschist to granulite grade from SW to NE and towards the contact with the granite over a distance of ~10 km (Clarke *et al.*, 1990; Vernon *et al.*, 1990; Collins & Vernon, 1991; Greenfield *et al.*, 1998). This reflects a high geothermal gradient of 75°C per vertical kilometre (Vernon *et al.*, 1990). The strong temperature increase across the sequence (~500–810°C, Greenfield *et al.*, 1998; White *et al.*, 2003) is accompanied by a small pressure increase (from 2·3–2·8 to 3·3–4·0 kbar, White *et al.*, 2003). The metamorphic sequence has been classically subdivided into a number of zones (Zones 1–5, Fig. 1a) of progressively increasing grade and degree of partial melting (Vernon *et al.*, 1990; Greenfield *et al.*, 1996, 1998). Zone 1 lacks evidence of melting and is characterized by low-grade muscovite quartz schists. Zone 2 is defined by the sub-solidus breakdown of muscovite to andalusite and K-feldspar (Zone 2a) and then by localized vapour-present melting (Zone 2b). The main rock assemblage is characterized by andalusite, cordierite and K-feldspar, with sillimanite appearing in the high-grade portion of the zone (Zone 2c). Metasediments in Zone 3 are migmatites that contain spinel, sillimanite, cordierite and K-feldspar, with occasional garnet. In Zone 4 the migmatites may additionally contain garnet and/or orthopyroxene. In Zone 5 the main rock type is a diatexite with biotite, cordierite and plagioclase, which is a physical mixture of migmatitic pelitic and psammitic rocks injected by magma from the granite. This simplified classification in zones is, however, complicated by the layered nature of the sequence and the reactions occurring in the different bulk rocks (White *et al.*, 2003). A comprehensive documentation of the metamorphic reactions and conditions has been given by White *et al.* (2003), who estimated peak metamorphism at around 800°C and 3·3–4·0 kbar. Whereas in the lower part of Zone 2 muscovite + quartz broke down to form

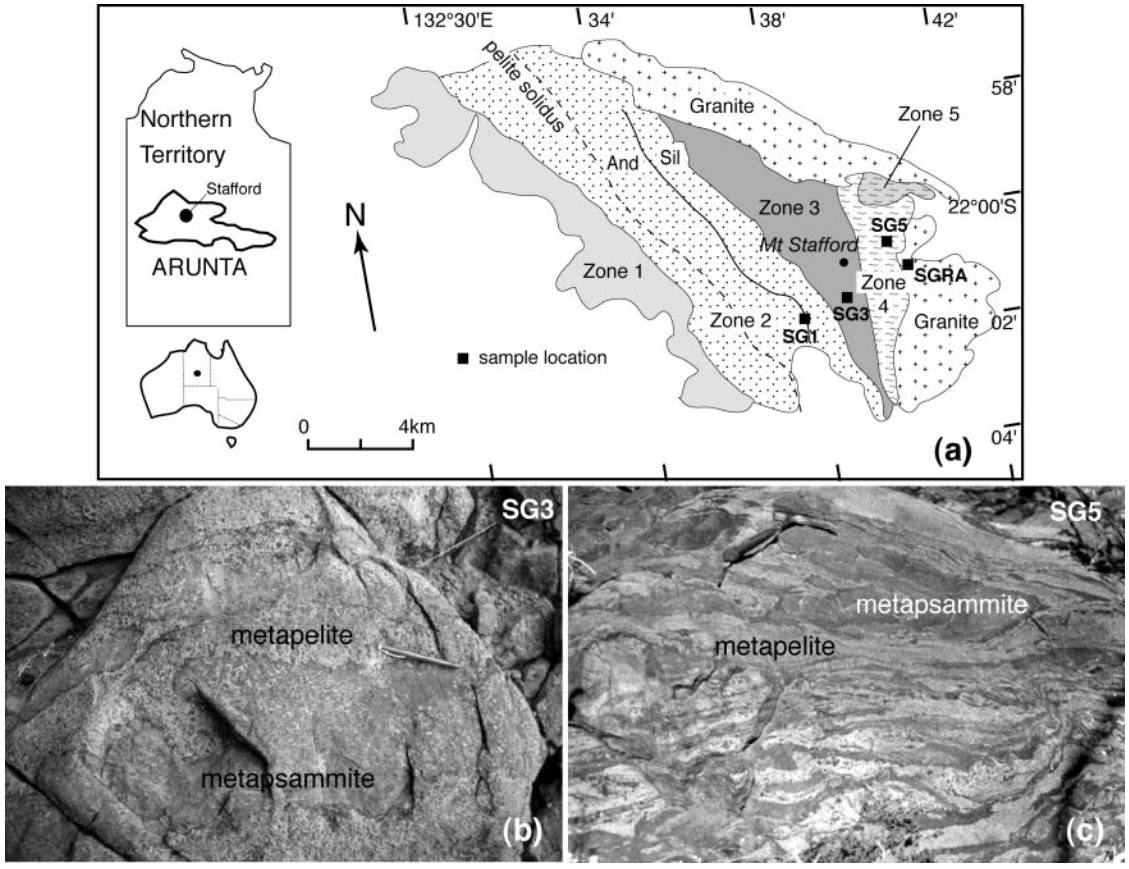

Fig. 1. (a) Schematic geological map of the Mount Stafford area [modified after Greenfield *et al.* (1998)] showing sample locations and metamorphic zones. (b) Field photograph of granulitic migmatites from locality SG3: the migmatitic texture is superimposed on the original sedimentary layering. Light layers (sample SGL3) and dark layers (sample SGP3) probably mimic the original pelitic–sandy banding. (c) Field photograph of granulites from locality SG5: the degree of partial melting is higher than in the lower-grade samples and the rock is a schlieren migmatite composed of a diatexite matrix (sample SGL5) with ribbons or lenses of cordierite-rich material (sample SGM5).

K-feldspar-bearing assemblages via sub-solidus dehydration reactions, a slightly higher grade (Zone 2b) melting began in the andalusite stability field, an unusual occurrence (Clarke *et al.*, 2005). The wet pelite solidus can intersect the andalusite–sillimanite transition if the Pattison (1992) Al_2SiO_5 polymorph triple point is used; in this case, andalusite and silicate melt can coexist at pressures of 2–2·5 kbar (Cesare *et al.*, 2003). Overall, the melting history at Mount Stafford is controlled by a series of biotite breakdown reactions experienced by the different rock types (metapsammites vs metapelites) at slightly different conditions over a P–T range and according to bulk-rock composition (White *et al.*, 2003). Thus, the banded nature of the protolith controls the rock's texture and the degree of melting at any given metamorphic grade. Compositional heterogeneity also controls the assemblages and the presence or absence of key minerals (e.g. garnet, orthopyroxene, aluminium silicate), and can produce micro-domains with different parageneses (White *et al.*, 2003). Melt mobilization over large distances appears to be limited, with most rocks containing the expected proportion of leucosome (White *et al.*, 2003). This is confirmed by the relatively constant bulk-rock composition of metapelites and metapsammites across the various zones (Greenfield *et al.*, 1996).

The Mount Stafford Beds appear to be equivalent to the more geographically widespread Lander Rock Beds, which occur in the south and NW of Mount Stafford. The Lander Rocks Beds have long been thought to have been deposited at ~1870 Ma (Blake & Page, 1988). However, more recent detrital zircon analysis suggested deposition after 1838 Ma (Vry *et al.*, 1996). The intrusion of the Mount Stafford granite has previously been estimated at 1818 ± 15 Ma through dating of magmatic zircon overgrowths (Collins & Williams, 1995). Relationships between granite intrusion and high-grade metamorphism are complex: (1) the granite cuts the mapped metamorphic isograds (Clarke *et al.*, 1990; Collins & Williams, 1995; Greenfield *et al.*, 1996), and itself has as a metamorphic aureole (Collins & Vernon, 1991; Collins & Williams, 1995); (2) the diatexite formed during metamorphism has a

gradational contact with the northern part of the granite (Clarke *et al.*, 1990; Greenfield *et al.*, 1996); (3) xenoliths of metamorphic country rocks are contained in the granite (Collins & Williams, 1995). In summary, the overall picture is one of interrelated metamorphism and magmatism (Vernon *et al.*, 1990; Collins & Vernon, 1991).

METHODS

The major element composition of garnet was determined on a JEOL 6400 SEM (Electron Microscopy Unit, ANU) and on a Cameca SX100 electron microprobe (EMP) using an acceleration voltage of 15 kV and a beam current of 1 and 10 nA, respectively. Garnet element mapping was performed on the Cameca SX100 with a voltage of 15 kV, current of 150 nA, a focused beam, 5 μm steps and a dwell time of 100 ms. Ca Kα was measured on a PET crystal and Y Lα on a TAP crystal.

Zircon and monazite grains were prepared as mineral separates mounted in epoxy and polished to expose the grain centres. Garnet was analysed in polished thin sections. Trace element analyses were performed by laser ablation–inductively coupled plasma mass spectrometry (LA-ICPMS) at the Research School of Earth Sciences (RSES) using a pulsed 193 nm ArF excimer laser with 100 or 70 mJ energy at a repetition rate of 5 Hz (Eggins *et al.*, 1998) coupled to an Agilent 7500 quadrupole ICPMS system. During the time-resolved analysis of minerals, the contamination from inclusions, fractures and zones of different composition was detected by monitoring several elements and integrating only the relevant part of the signal. A spot size of 23 μm (zircon and monazite), and 83 or 142 μm (garnet) was used. External calibration was performed relative to NIST 612 glass using the concentrations given by Pearce *et al.* (1997). Internal standards were Ca and Si for garnet, as measured by EMP, and stoichiometric Si and Ce for zircon and monazite, respectively.

Cathodoluminescence (CL) investigation of zircon was carried out at the Electron Microscope Unit, Australian National University, with an Hitachi S2250-N scanning electron microscope working at 15 kV, ~60 μA and ~20 mm working distance. Back-scattered electron (BSE) images were obtained with a Cambridge S360 scanning electron microscope using a voltage of 20 kV, current of ~2 nA and a working distance of 15–20 mm.

U–Th–Pb analyses were performed using SHRIMP I and II at the RSES. Instrumental conditions and data acquisition for zircon analysis were generally as described by Compston *et al.* (1984). For monazite, energy filtering was used to eliminate the interference on ^{204}Pb, as described by Rubatto *et al.* (2001). The data were collected in sets of six or seven scans throughout the masses. The measured ^{206}Pb/^{238}U ratio was corrected using reference zircon from a gabbro of the Duluth Complex in Minnesota (AS3, 1099 Ma, Paces & Miller, 1993) and reference monazite from the Thompson mine (1766 Ma). A zircon of known composition (SL 13) was used to determine the U content of zircon. The data were corrected for common Pb on the basis of the measured ^{204}Pb, as described by Compston *et al.* (1984). The low common Pb content of both standard and unknowns indicated that the common Pb was mainly surface-derived and instrumental background. Therefore, the common Pb composition was assumed to be that of Broken Hill galena, which approximates the laboratory common Pb background at the RSES. Ages were calculated using the software Isoplot/Ex (Ludwig, 2000). Isotopic ratios and single ages are reported with 1σ error, whereas mean ages are given at the 95% confidence level (c.l.).

SAMPLE DESCRIPTION

Several pairs of inter-layered samples were collected at different metamorphic grades in the prograde sequence. Across the Mount Stafford terrane, melting did not lead to the formation of discrete melanosomes and leucosomes at the sample scale (Greenfield *et al.*, 1996; White *et al.*, 2003). Instead, the banded nature of the rocks at all grades mostly reflects the original sedimentary layering [the 'bedded migmatites' of Greenfield *et al.* (1998)]. On an outcrop scale, at grades above the solidus, metapelites have generally melted to a greater extent than inter-layered metapsammites (e.g. White *et al.*, 2003). Three pairs of samples were investigated in detail; each comprises a metapelite, in which a higher degree of melting was reached, and the associated metapsammite, in which generally melting was less pronounced. Sample locations are shown in Fig. 1a and assemblages are given in Table 1.

SGL1 is a metapelite and SGP1 a nearby (<1 m) metapsammite, which form decimetre-scale bands that reflect the original layering of the sedimentary precursor. SGLI has a weak foliation defined by biotite and sillimanite, and also contains deformed quartz and cordierite. The rock also contains skeletal garnet with inclusions of biotite, sillimanite and ilmenite. The presence of garnet at this low metamorphic grade [Zone 2 of Greenfield *et al.* (1998)] is unexpected. The crystals appear to be corroded, are deformed along the foliation, and thus are in a different textural setting from the late symplectitic garnet described by Clarke *et al.* (1990). The composition of this garnet is also different from the garnet found in higher-grade samples: it is poorer in CaO (0·3–0·5 vs 1·0–1·1 wt %) and in MnO

Table 1: *Sample description and age summary*

	Rock type	Zone	*P* (kbar) and *T* (°C)*	Assemblage	Zircon age (Ma)	Monazite age (Ma)
SGL1	metapelite	Zone 2b–c	~2·5, ~650	Kfs–qtz–crd–bt–sill–spn–(grt)–opm–zrn–mnz	n.a.	1805 ± 4
SGP1	metapsammite	Zone 2b–c	~2·5, ~650	Kfs–qtz–crd–bt–sill–spn–opm–zrn–mnz	1853–2063c	1805 ± 3, 1819–1883c
SGL3	metapelite	Zone 3	3·3–4·0, 775–785	Kfs–qtz–crd–bt–spn–opm–zrn–mnz	1802–2515c	1797 ± 5
SGP3	metapsammite	Zone 3	3·3–4·0, 775–785	Kfs–qtz–pl–crd–bt–grt–opx–opm–zrn–mnz	1818–2560c	1790 ± 7, 1947–2448c
SGL5	metapelite	Zone 4	~4·0, 800–810	Kfs–qtz–pl–crd–bt–grt–spn–opm–zrn–mnz	1797 ± 6, 1854c, 2167c	1800 ± 5 (1803 ± 8c, 1798 ± 6r)
SGM5	metapsammite	Zone 4	~4·0, 800–810	Kfs–qtz–crd–bt–grt–opx–spn–opm–zrn–mnz	1792 ± 9	1806 ± 6 (1811 ± 7c, 1801 ± 10r)
SGRA	granite			Kfs–qtz–crd–pl–bt–spn–opm–zrn–mnz	1805 ± 3, 1865c	1802 ± 3

**P–T* estimates given are according to the zones of Greenfield *et al*. (1998) and White *et al*. (2003), and are not calculated directly from these samples.
Mineral abbreviations are according to Bucher & Frey (1994); c, r, ages corresponding to cores and rims, respectively; n.a., not analysed.

(0·35–0·75 vs 1·0–1·6 wt %). The same rock contains large sillimanite blasts wrapped by a fibrolite and biotite fabric; although the garnet and the sillimanite blasts are never in contact, both minerals could belong to the same paragenesis. SGP1 is a fine-grained, light-coloured metapsammite poor in biotite (<10%) and rich in quartz and K-feldspar. Other rocks from the same outcrop contain andalusite: this places the sample at the boundary of Zones 2b and 2c (Fig. 1), corresponding to the andalusite–sillimanite transition according to the scheme of Greenfield *et al.* (1998). Metamorphic conditions at this boundary are estimated at T ~650°C and P ~2·5 kbar (Greenfield *et al.*, 1998; White *et al.*, 2003).

SGL3 corresponds to a metapelite and SGP3 is a nearby metapsammite that shows evidence of limited melting. Both samples are sillimanite absent, as are similar rocks described elsewhere in Zones 3 and 4 (Greenfield *et al.*, 1998; White *et al.*, 2003). They were collected in the area where partial melt was widespread (15–25% in metapelites according to previous estimates; Greenfield *et al.*, 1998; White *et al.*, 2003), but still located in bands according to the sedimentary layers (Fig. 1b). Cordierite and spinel symplectites are common in the metapelite. In contrast, garnet and orthopyroxene are present in the metapsammite as peritectic products of biotite dehydration melting reactions. The development of garnet- and orthopyroxene-bearing assemblages at Mount Stafford is consistent with P–T conditions of 750–800°C and 3–4 kbar (White *et al.*, 2003).

SGL5 and SGM5 were collected closer to the granite (Zone 4, Fig. 1), where the peak temperature conditions were ~800°C (Greenfield *et al.*, 1998; White *et al.*, 2003), and a higher percentage of partial melting occurred (20–30% in metapelites; Greenfield *et al.*, 1998; White *et al.*, 2003). In this area, the regular banded texture and layers of metapelites and metapsammites seen at lower grades is less evident, and the rocks are schlieren migmatites composed of a diatexite matrix (SGL5) with ribbons or lenses of darker material (SGM5, Fig. 1c). Garnet is present in both SGM5 and SGL5 and contains frequent biotite inclusions, suggesting that it formed at the expense of biotite. Cordierite is significantly more abundant in SGM5 (~60% by volume) than in the diatexite SGL5. Rare, interstitial orthopyroxene is present in SGM5.

Sample SGRA represents the Mount Stafford granite and was collected within the eastern part of the body. The rock is primarily composed of K-feldspar and quartz with very minor plagioclase. Biotite and cordierite occur locally, partly corroded or rimmed by feldspar, and appear to be xenocrysts. Spinel occurs as aggregates or trails in the interstices between feldspars.

ZIRCON AND MONAZITE PETROGRAPHY AND GEOCHRONOLOGY

SGL1–SGP1

Monazite was separated from both lower-grade samples, SGL1 and SGP1. Monazite grains are yellow, clear and subhedral. In BSE images (Fig. 2), monazite from sample SGL1 generally shows dark cores of irregular shape surrounded by brighter, homogeneous rims. SHRIMP dating did not identify any significant age difference between cores and rims (Electronic Appendix 1, available at http://www.petrology.oxfordjournals.org): 12 analyses out of 13 yielded an average $^{207}Pb/^{206}Pb$ age

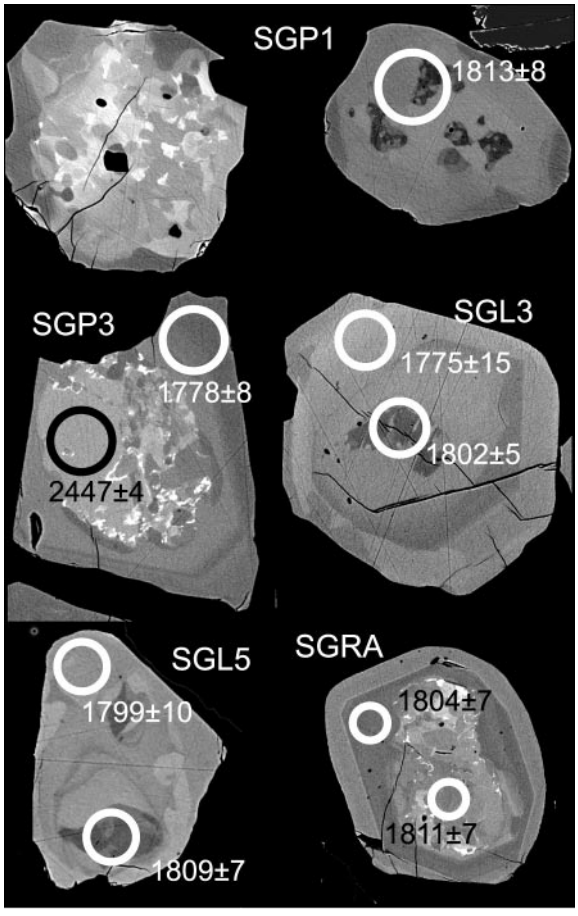

Fig. 2. Back-scattered electron image of monazite grains from different samples. Metamorphic grade increases from top to bottom. At lower grade, monazite grains preserve a patchy zoning that, when analysed, yielded pre-1800 Ma ages. In contrast, from sample SGL3 onwards no difference in age was detected between the domains, although a tendency to older cores and younger rims is observed in a number of samples. Circles representing SHRIMP analyses are 20 μm in diameter.

of 1805 ± 4 Ma (MSWD = 1·8; 95% c.l., Fig. 3). One discordant analysis yielded a slightly older age and was thus excluded from the calculation.

In the metapsammite SGP1, the BSE imaging revealed a more complex texture, with different zoning patterns varying from weak oscillatory, to patchy, to homogeneous rims on dark cores (Fig. 3). The complexity in the zoning is partly confirmed by U–Pb dating; the ages scatter between 1797 and 1883 Ma (Electronic Appendix 1, http://www.petrology.oxfordjournals.org). However, zoning and ages do not necessarily correlate. Two of the older ages (1878 and 1871 Ma) were measured on the only monazite grain with oscillatory zoning that was dated, which also has significantly higher Th/U. Another age of 1883 Ma was measured on a patchy-zoned domain; however, similarly zoned domains in other grains yielded younger ages. Of the 17 analyses, seven were excluded because they were significantly older, high in common Pb and/or discordant. The remaining 10 analyses yielded an average $^{207}Pb/^{206}Pb$ age of 1805 ± 3 Ma (MSWD = 1·6; 95% c.l., Fig. 3). The other analyses scatter in age between 1819 and 1883 Ma ($^{207}Pb/^{206}Pb$ ages within ±10% discordance) and correspond to domains with commonly lower U and higher Th/U.

Zircon was recovered only from metapsammite SGP1. The crystals are mainly euhedral with rounded edges, but a number of crystals are fragments. They are brownish with abundant inclusions. The internal zoning in CL is highly variable, from bright oscillatory to dark domains where no zoning pattern can be distinguished. Commonly, a core–rim structure was observed. SHRIMP analyses were performed exclusively on dark rims, which were considered more likely to have formed during anatexis. Some of these rims have Th/U as low as 0·01, which, together with the poor zoning, might suggest a metamorphic origin (e.g. Williams *et al.*, 1996; Rubatto *et al.*, 2001). The $^{207}Pb/^{206}Pb$ ages range between 1853 and 2063 Ma (Electronic Appendix 1, http://www.petrology.oxfordjournals.org). The major components of this zircon population are five analyses on three grains at 1856 ± 3 Ma and five others at 1873 ± 4 Ma. None of the zircon appears to have grown during the event that produced the 1805 Ma monazite.

SGL3–SGP3

Both samples contain yellow, clear monazite grains that preserve some crystal faces, but are generally not euhedral. In BSE images monazite displays a core–rim texture with dark cores with patchy zoning, and homogeneous brighter rims (Fig. 2). The zoning correlates with the U content of the monazite (zones with higher BSE emission have higher U content) and with Th/U (core = 2, rims >10; see also the trace element section). The analyses (except for two) were performed on rims because cores are generally smaller than 25 μm. All 10 analyses, including the two rim analyses, form a tight group with an average $^{207}Pb/^{206}Pb$ age of 1797 ± 5 Ma (MSWD = 0·95; 95% c.l., Fig. 3).

In metapsammite SGP3, monazite is abundant in the matrix and occasionally included in garnet. Garnet in this rock is highly skeletal and contains few inclusions. In BSE images monazite displays a strong core–rim structure, with large patchy-zoned cores and unzoned rims (Fig. 2). As inheritance was suspected, most of the analyses were performed on the rims and yielded ages with an average $^{207}Pb/^{206}Pb$ of 1790 ± 7 Ma (MSWD = 0·55; 95% c.l., Fig. 3). One analysis has a significantly younger age and was excluded from the calculation. The analyses on cores or overlapping core and rim (some of the rims were too small) have, compared with the

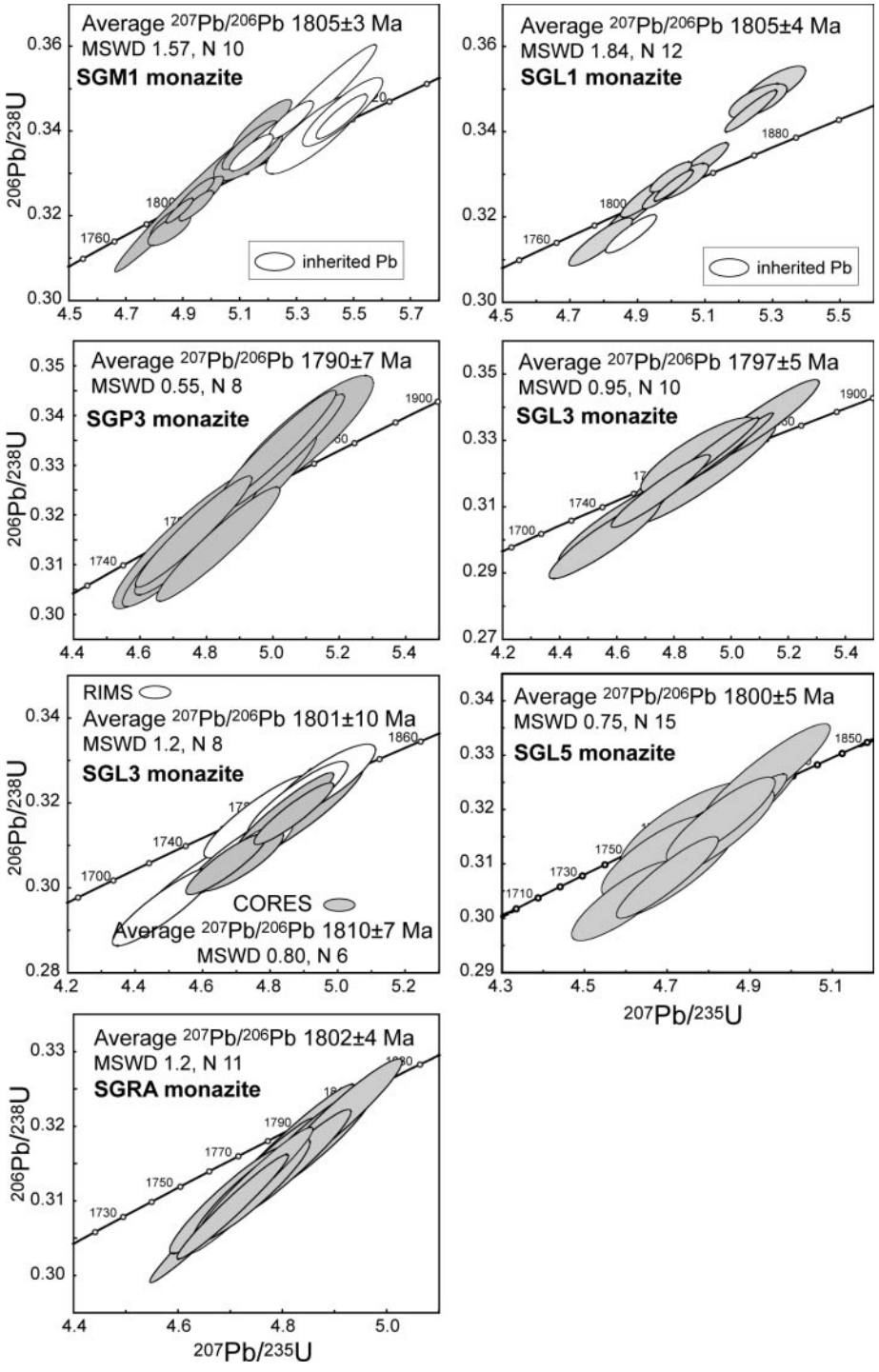

Fig. 3. Concordia diagram representing SHRIMP analyses of monazite from Mount Stafford. Ellipses represent 2σ errors. Average ages are given at 95% c.l.

rims, higher U, lower Th/U and older ages, up to 2448 ± 4 Ma for analysis 1.2, which corresponds to a core (Electronic Appendix 1, http://www.petrology.oxfordjournals.org). Monazite contains inclusions of metamorphic minerals such as cordierite and biotite.

In metapelite SGL3 the majority of zircon crystals are clear, pink and euhedral. In sample SGP3, a large number of crystals are rounded and with a rough surface. In this sample a large fraction (~70% of grains) is dark, non-transparent, red to brown and rounded.

Fig. 4. Cathodoluminescence images of zircon crystals from various samples. In the intermediate-grade sample SGP3 unzoned zircon rims yield a pre-1800 Ma age and are interpreted as predating migmatization. In the associated melt-rich metapelite SGL3 similar unzoned rims yield the age of metamorphism. Zircon from the high-grade rock SGL5 and the granite SGRA are very similar and have the same age. Circles representing SHRIMP analyses are 25 μm in diameter.

CL imaging revealed that in both samples the internal oscillatory zoning pattern is truncated at the surface (Fig. 4), indicating that abrasion or corrosion of the zircon occurred after formation. The zircons commonly show a core–rim structure in CL images. A significant number of crystals, more abundant in sample SGP3, are dark in CL, and hardly any zoning can be distinguished in these grains. They probably correspond to the dark, non-transparent, coloured crystals observed in transmitted light. This zircon type contains inclusions of major rock-forming minerals (K-feldspar, biotite, quartz, plagioclase and ilmenite) as well as uncommon accessory minerals such as xenotime, U and Pb oxides, and small grains of light rare earth element (LREE) phosphate(s).

SHRIMP analyses were concentrated in the outer rims of the crystals and in the dark domains, which, because of their outer position and/or poor zoning were considered more likely to have formed during metamorphism. The pattern of ages obtained is similar in both samples (Electronic Appendix 1, http://www.petrology.oxfordjournals.org). They scatter between 1802 Ma (1818 Ma in SGP3) and ~2500 Ma with some clustering at around 1820–1840–1870 Ma (average of two samples: 1823 ± 5 Ma, $n = 8$; 1842 ± 6 Ma, $n = 6$; 1871 ± 5 Ma, $n = 5$). Low Th/U values were measured for one of the domains in each age group. Sample SGL3 has a younger component represented by three analyses between 1802 and 1805 Ma. The analyses around 1805 Ma all have low Th/U (0·05–0·01) whereas in both samples the majority, but not all, of the older ages correspond to domains with Th/U >0·1. In sample SGP3 zircon domains dated at ~1820 Ma ($^{207}Pb/^{206}Pb$ age more than 95% concordant) contain inclusions of biotite, whereas cordierite is present at the boundary between a 1820 and 1860 Ma domain, both domains having Th/U >0·1.

SGL5–SGM5

Monazite in sample SGL5 has been observed as inclusions in garnet and in the matrix (Fig. 5). Monazite from both samples has similar characteristics: they are clear, light yellow, and mainly euhedral. The crystals display a patchy-zoned core surrounded by a more homogeneous or oscillatory-zoned rim (Fig. 2). Monazite cores are also distinguished by a Th/U ratio below 10, whereas the rims have Th/U of the order of 30–50 (see trace element section, below). In both samples, there is a tendency for the monazite rims to yield lower ages than the cores, but the difference cannot be resolved with the present analytical precision. However, on the basis of the BSE information the 15 analyses from SGL5 monazite yielded an age of 1803 ± 8 Ma for the cores, and 1798 ± 6 Ma for the rims (mean age 1800 ± 5 Ma). Monazite in sample SGM5 yielded a core age of 1811 ± 7 Ma and a rim age of 1801 ± 10 (mean age 1806 ± 6 Ma).

Zircon crystals have similar features in both samples: they are clear, pink to brownish, elongated, and mainly euhedral. The CL investigation confirmed this similarity between the two samples: the zircon crystals generally have a composite core with various oscillatory-zoned patterns that commonly cross-cut each other (Fig. 4). The core is commonly surrounded by a homogeneous overgrowth that can range in thickness from a few microns to 50 μm on some crystal tips. The main difference between the samples is that in the diatexite SGL5 the overgrowths are more abundant and generally thicker. Isotopic measurements were mainly carried out on the overgrowths. Of the 17 analyses on overgrowths in sample SGL5, one with particularly high common Pb yielded a younger age (1754 ± 16 Ma). The remaining 15 analyses are from domains with low Th/U (0·12–0·07) and define a tight cluster with an

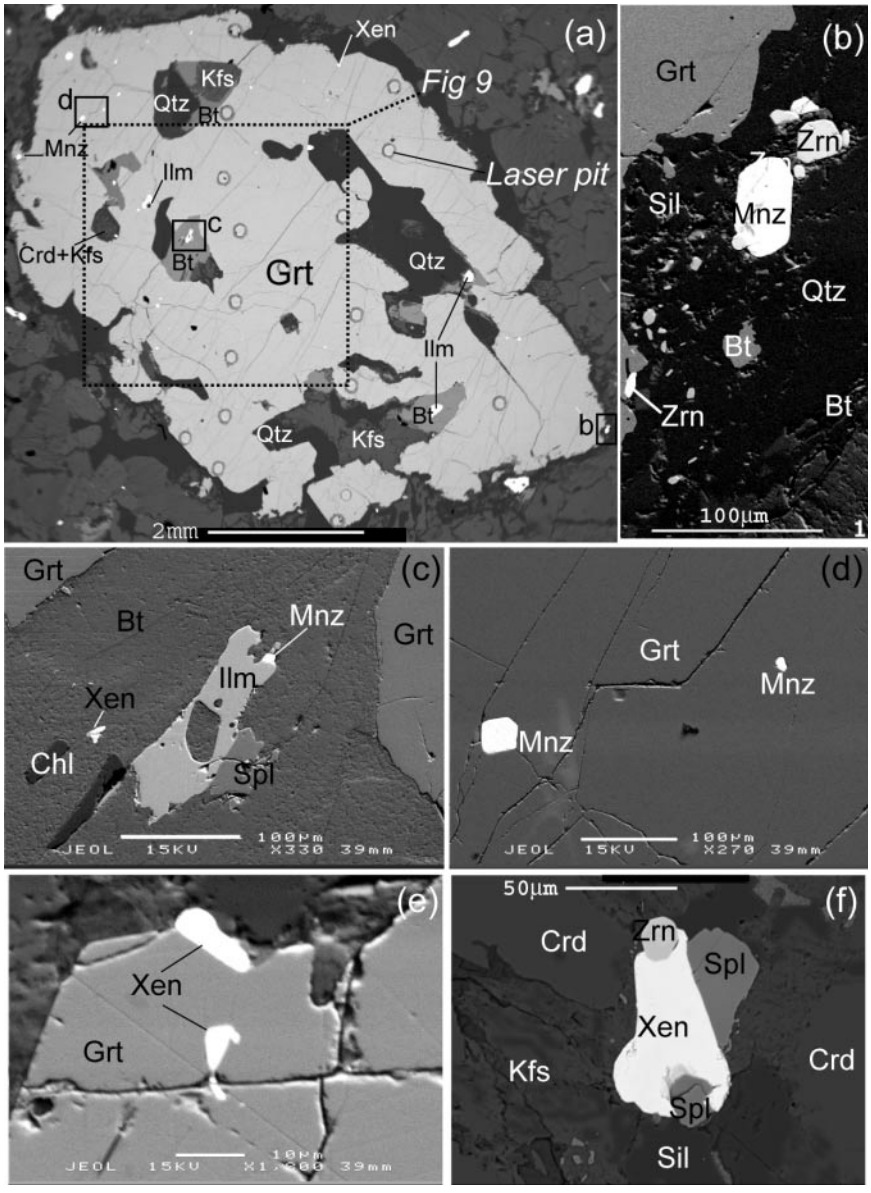

Fig. 5. BSE images of textures involving garnet and U–Pb accessory minerals in thin section SGL5. (a) Large garnet (Grt) porphyroblast in SGL5 with a number of inclusions of U-rich minerals and other phases (Bt, biotite; Crd, cordierite; Kfs, K-feldspar; Ilm, ilmenite; Mnz, Monazite; Qtz, quartz; Sil, sillimanite; Zrn, zircon; Xen, xenotime). The large dotted square indicates the area mapped in Fig. 9, whereas the small squares numbered b–d refer to other images in this figure. (b) Monazite and zircon in the matrix close to the garnet rim. (c) Monazite and xenotime within biotite included in garnet. (d) Monazite included in the garnet rim. (e) Xenotime included in the garnet rim [garnet grain different from that in (a)]. (f) Xenotime and zircon in the rock matrix. Contrast and brightness have been adjusted and are not constant from one image to the other.

average $^{207}Pb/^{206}Pb$ age of 1797 ± 6 Ma (Fig. 6). Two analyses on zircon cores yielded 1854 ± 11 Ma and 2167 ± 11 Ma and are characterized by a higher Th/U of 0·9 and 0·5, respectively.

For sample SGM5, only seven analyses were possible on the overgrowths because of their small size and low abundance. U, Th and Th/U compositions are similar to those of the overgrowths in sample SGL5 (Electronic Appendix 1, http://www.petrology.oxfordjournals.org). The analyses cluster together and define a $^{207}Pb/^{206}Pb$ age of 1792 ± 9 Ma (Fig. 6), which is indistinguishable from that of the zircon overgrowths in SGL5.

SGRA

The granite contains large monazite crystals that are clear, yellow and mainly euhedral. In BSE images, they have a zoning pattern characterized by a somewhat chaotic or homogeneous core, which is surrounded by a

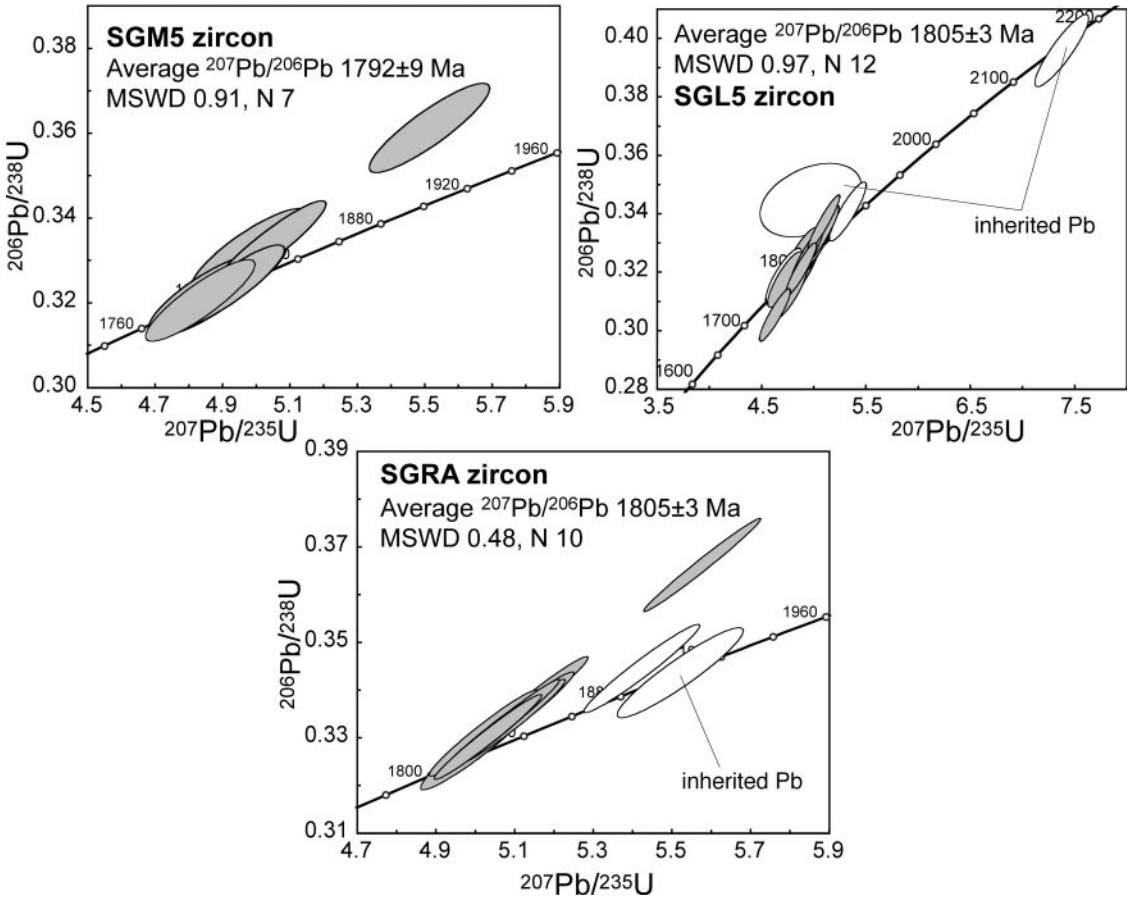

Fig. 6. Concordia diagram representing SHRIMP analyses of zircon from Mount Stafford. Ellipses represent 2σ errors. Average ages are given at 95% c.l.

rim with oscillatory growth zoning (Fig. 2). This kind of zoning is consistent with a magmatic origin for the monazite rims. SHRIMP dating revealed no differences in age between monazite cores and rims. Twelve analyses define an average $^{207}Pb/^{206}Pb$ age of 1802 ± 3 Ma (Fig. 3), which is indistinguishable from the age of the metamorphic zircon rims.

Zircon is very similar in aspect to that of the diatexite SGL5. The CL features are also similar, with large unzoned overgrowths on oscillatory-zoned cores (Fig. 4). Ten dated overgrowths yielded $^{207}Pb/^{206}Pb$ ages that tightly cluster around an average of 1805 ± 3 Ma (Fig. 6). A single core measured yielded an older age of 1865 ± 5 Ma. This analysis is characterized by a higher Th/U (0·13) than measured for the overgrowths (0·01–0·04).

TRACE ELEMENT COMPOSITION

Trace element composition of zircon was obtained for sample pairs SGP3–SGL3 and SGL5–SGM5, whereas monazite data were also collected for samples SGL1 and SGP1, to test their homogeneity and correlate the chemical variation with age. For the interpretation of zircon and monazite response to metamorphism it is essential that only domains that formed during metamorphism are considered and not potential inherited domains. The petrography and dating provided evidence that domains with different appearances display indistinguishable metamorphic ages. Here we will investigate whether or not these domains have different trace element characteristics. The trace element data are subdivided into the following three categories: (1) inherited domains (>1820 Ma); (2) metamorphic cores or inner domains (~1800 Ma); (3) metamorphic rims (~1800 Ma).

The trace element composition of garnet was also measured because garnet is the major phase rich in trace elements, particularly heavy rare earth elements (HREE), present in this rock. Biotite, cordierite and feldspar are generally poor in REE and Y, although they might contain some large ion lithophile elements (LILE) and LREE (e.g. Bea *et al.*, 1994; Yang *et al.*, 1999; Yang & Rivers, 2002; Buick *et al.*, 2006).

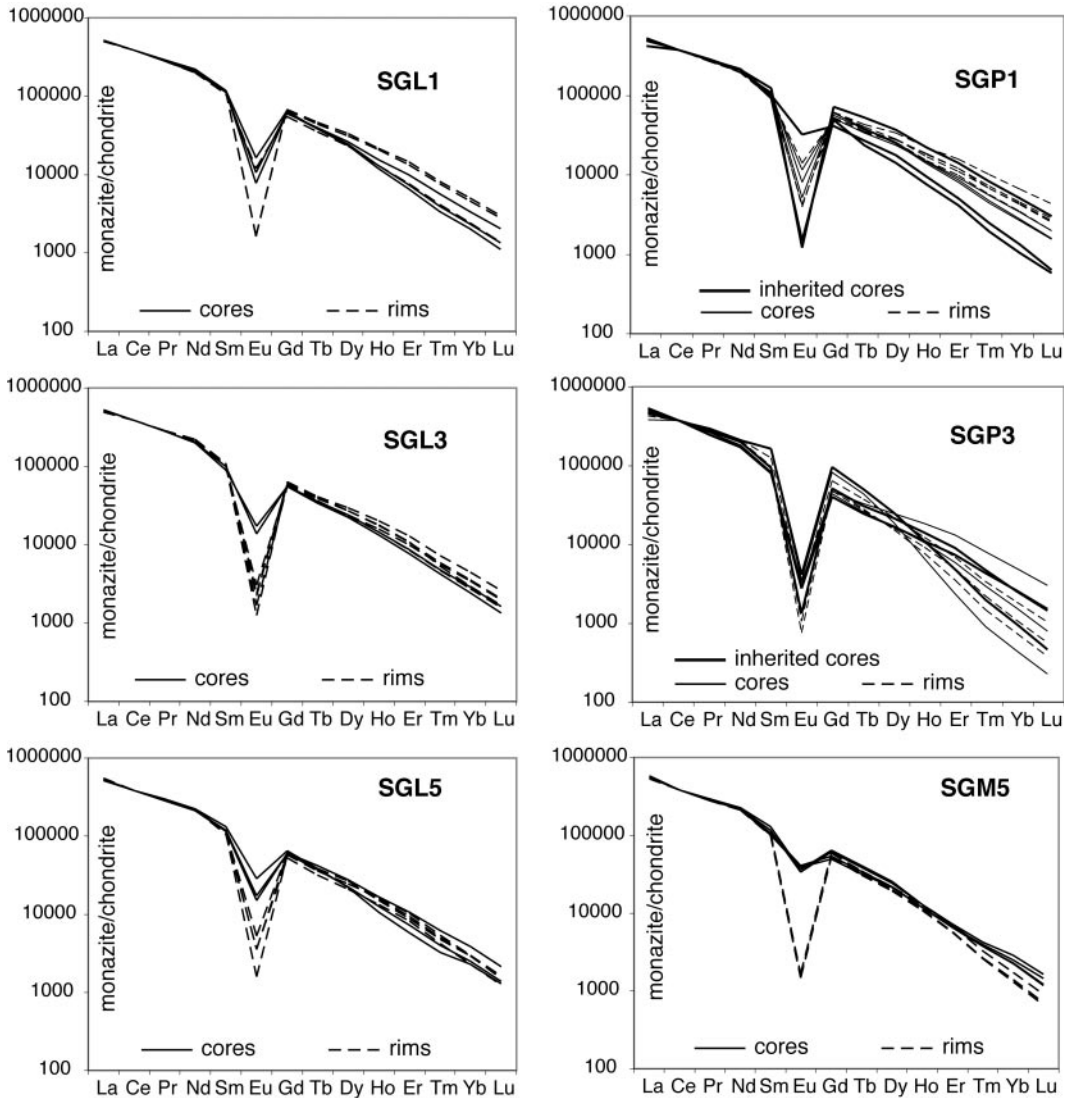

Fig. 7. Monazite rare earth element patterns. Inherited cores, metamorphic cores and metamorphic rims are distinguished. Chondrite normalization is according to Sun & McDonough (1989). (See text for details.)

Monazite

The chondrite-normalized (Sun & McDonough, 1989) trace element pattern of monazite is characterized by a strong relative enrichment in LREE (500 000–550 000 times chondrite for La, a major element in monazite) with a progressive and smooth decrease in normalized abundance toward the HREE, and generally a negative Eu anomaly (e.g. Bea *et al.*, 1994; Hermann & Rubatto, 2003; Buick *et al.*, 2006). Monazite trace element data for the Mount Stafford samples are plotted in Fig. 7 and average compositions are given in Electronic Appendix 2 (http://www.petrology.oxfordjournals.org).

Trace element analysis of monazite from samples SGL1 and SGP1 revealed a difference between the metamorphic core and rim observed in BSE images, which yield the same U–Pb age of 1805 Ma (no inherited monazite cores were analysed). Monazite rims generally have a more marked negative Eu anomaly and a pattern less depleted in HREE when compared with the dark or patchy zoned cores. The difference in HREE abundances is particularly marked in metapsammite SGP1. Inherited cores older than 1820 Ma have variable compositions with a strong relative HREE depletion.

For monazite in SGL3, which has a uniform U–Pb isotopic composition and hence the observed core–rim zoning is entirely metamorphic, the measured trace elements show differences that correlate with the zoning observed in BSE images. In particular, analyses from the dark cores in BSE images differ from the unzoned rims

in having a less pronounced negative Eu anomaly (Eu/Eu* = 0·18–0·25 vs 0·02–0·04 in rims), lower contents of Y, Ti and Th, and higher U contents.

Monazite in the metapsammite at the same metamorphic grade, SGP3, preserves a variety of zoning patterns and inherited U–Pb components in the cores of the crystals. There is also a large variation in the trace element content, particularly in the middle REE (MREE) to HREE. It appears that the composition of the monazite cores dated at ~1800 Ma varies over a wider range (Gd/Lu 15–360) than that of the rims (Gd/Lu 62–139); however, the two domains have only a slight difference in Eu/Eu*, and similar Th and U contents. A variety of compositions are also observed in the inherited cores (1947–2448 Ma).

In samples SGL5 and SGM5 some difference in age, although not completely resolvable, was detected between monazite cores and rims. For sample SGL5 monazite trace element analysis revealed variations in Th/U and the extent of the negative Eu anomaly that can be generally correlated to the core–rim zoning. In the associated layer SGM5, the composition of monazite reflects the BSE zoning and the stronger age difference: dark, older cores are richer in U and poorer in Th, have a low Th/U ratio (5–13 vs 44–51 in the rim) and a smaller negative Eu anomaly with respect to the younger rims.

The different monazite domains from the granite are similar in REE contents with limited variations in degree of negative Eu anomaly (larger in the rims) and Th content (higher in the rims; Electronic Appendix 2, http://www.petrology.oxfordjournals.org).

Zircon

It has been widely documented that zircon generally has a chondrite-normalized REE pattern characterized by strong enrichment in HREE with respect to MREE, low abundance of LREE close to or below chondrite values, a negative Eu anomaly and a positive Ce anomaly (e.g. Heaman *et al.*, 1990; Hinton & Upton, 1991; Hoskin & Schaltegger, 2003). This is the case for magmatic zircon, but zircon formed in a metamorphic environment, particularly in sub-solidus conditions, can have different characteristics (e.g. Rubatto, 2002; Hoskin & Schaltegger, 2003).

Trace element analyses of zircon from Mount Stafford were mainly obtained from rims that yielded ages around 1800 Ma (Fig. 8 and Electronic Appendix 2, http://www.petrology.oxfordjournals.org). The composition of zircon rims from the two highest-grade samples, SGL5 and SGM5, is very similar. Both have patterns with strong enrichment in HREE relative to the MREE (Lu/Gd 25–70), negative Eu anomalies (Eu/Eu* 0·02–0·36) and positive Ce anomalies (1·8–8·1). The

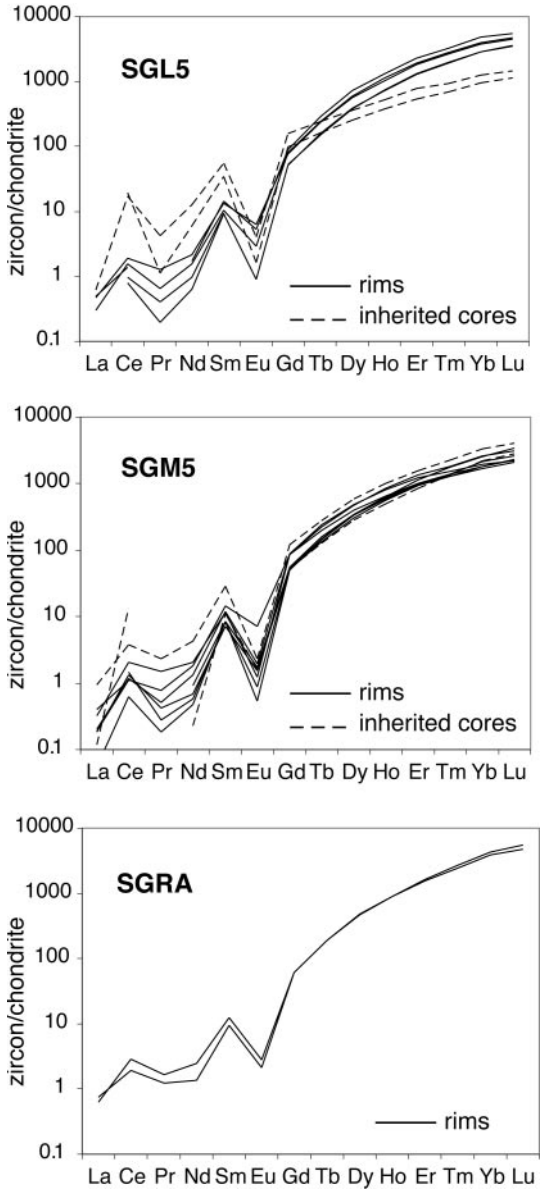

Fig. 8. Zircon rare earth element patterns. Dashed lines in SGL5 and SGM5 zircon represent inherited zircon cores. Chondrite normalization is according to Sun & McDonough (1989). (See text for details.)

zircon from SGL5 is slightly richer in HREE than its counterpart in SGM5 (Lu 87–136 vs 54–84 ppm). There is a variation in Eu anomaly from grain to grain, but the average is similar in both samples, as is Th/U. Two analyses were obtained for zircon cores in SGL5 and both are similar and clearly distinguishable from the rim: the former differ from the latter by a stronger positive Ce anomaly and negative Eu anomaly, weaker relative HREE enrichment, and higher Th and Th/U. One of the cores corresponds to an oscillatory zone

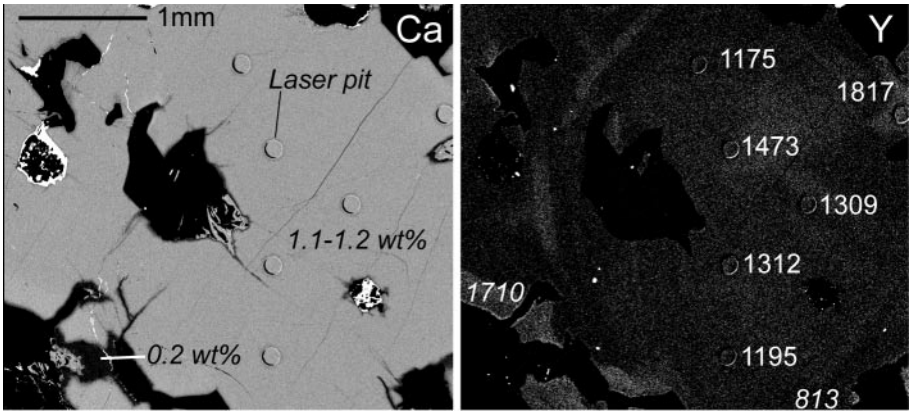

Fig. 9. Element mapping of a garnet crystal from SGL5. The zoning in Ca (small low-Ca rim) and Y do not match. A BSE image of the garnet is given in Fig. 5. (See text for comments.) The CaO content measured by EMP is reported in wt %. The Y map contains Y contents (ppm) measured by LA-ICPMS on the spots visible in the map; values in italics indicate measurements made on similar zones of the same grain, but outside the area mapped.

dated at 1854 ± 11 Ma. For SGM5 the two cores analysed are different and both can be distinguished from the rims because of higher Th/U (1·6 vs 0·03–0·1), and either larger Ce anomaly or higher LREE content.

The composition of the 1805 Ma zircon rims from the granite is similar to that measured in zircon rims from the high-grade granulites.

Garnet

Garnet from samples SGP3, SGM5 and SGL5 was analysed for major and trace elements (Electronic Appendix 3 and 4, http://www.petrology.oxfordjournals.org). The garnet is generally homogeneous in major elements; it is rich in FeO (almandine 80–85%) and poor in CaO and MnO (grossular 2·9–3·0%, spessartine 2·2–3·8%). In the highest-grade samples (SGL5 and SGM5), a thin, low-CaO domain (CaO 0·5 wt %) may be present along the grain rim or at the contact with inclusions or fractures (Fig. 7).

The trace element composition of the garnet is more complex. Y mapping (Fig. 9), although close to detection limits, shows that Y zoning is not necessarily related to Ca zoning and is more pronounced than any major element zoning. LA-ICPMS traverses across a number of garnet crystals (8–10 analyses spaced 700–900 μm for each garnet) were also measured (Fig. 10). EMP element mapping coupled with LA-ICPMS spot analysis was used to reconstruct the garnet trace element zoning of garnets from samples SGL5 and SGM5. Zoning mainly involves Ti, Y and the HREE and, to a lesser extent P, Zr and Hf. A zone of irregular shape, and richer in Ti, Y and the HREE, but generally poorer in P is visible in the centre of the garnet (hereafter referred to as the garnet core); its location and dimension can vary from garnet to garnet. It contains 80–100 ppm P, 190–240 ppm Ti, up to 2000 ppm Y, and 250–700 ppm Yb, varying from grain to grain. This Y-rich core gradually changes to an intermediate domain that is volumetrically the most important (hereafter referred to as the intermediate zone): P is around 140–200 ppm, Ti is 140–170 ppm, Y is ~500–1200 ppm and Yb is in the range 60–180 ppm. In one of the three garnet grains mapped, a Y-rich annulus of ~150 μm width is present in the intermediate part. However, because of its narrowness, no quantitative LA-ICPMS analyses are available for this annulus. A 200–250 μm wide Y-rich zone is present along most of the garnet rim (hereafter referred to as the garnet rim) at the contact with a variety of minerals (quartz, cordierite or feldspars). The rim is similar in composition to the core and has Ti, Y and Yb contents of 150–250 ppm, 1000–1800 ppm, and generally 400–650 ppm, respectively. There is some systematic variation in absolute trace element content between garnets from the two samples: SGP3 garnet is the lowest in trace element content, and SGM5 garnet is slightly lower than SGL5 garnet. Particularly for the two high-grade samples, this difference could partly be an artefact of sampling bias and/or the cut of the garnet investigated. Because of the small dimension of the low-Ca rim, no trace element analysis has been obtained for this domain.

In summary, trace element traverses across garnet have a W-shaped trend, with core and rim regions richer in Ti, Y and HREE. This W-shaped pattern is reproducible and is particularly marked in the higher-grade samples where the crystals are larger. Sample SGP3 has a weak W-shaped zoning, but this is more difficult to reconstruct because of the smaller size of the garnet and its highly skeletal nature. SGP3 garnet has

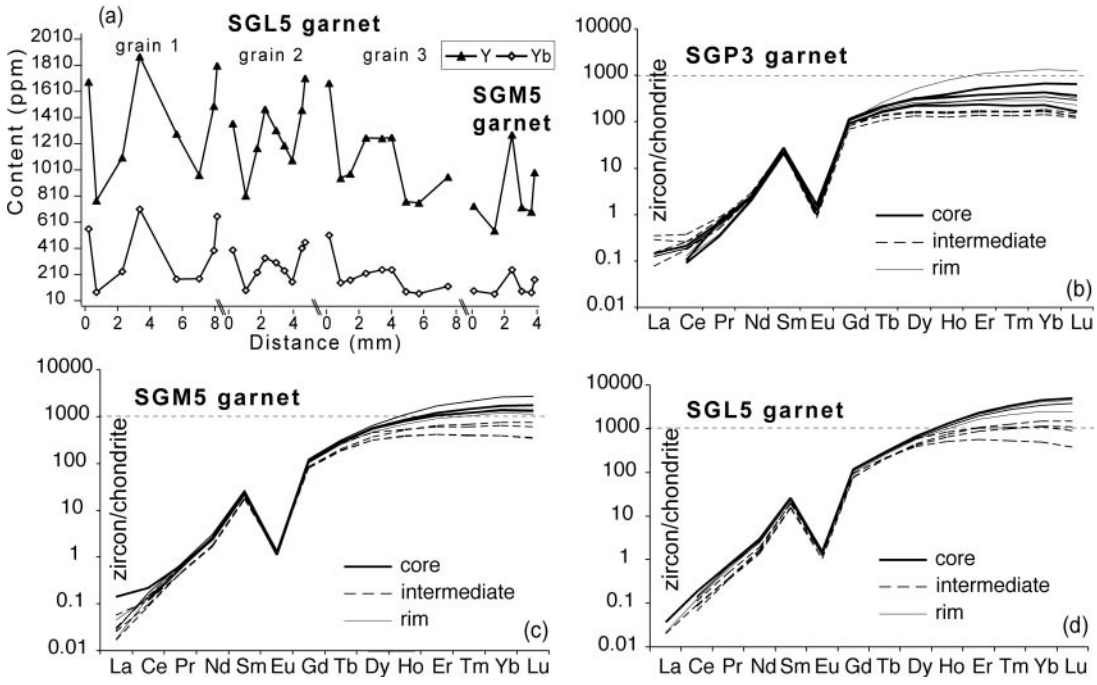

Fig. 10. Garnet trace element composition. (a) Y and Yb variation across three garnet grains of sample SGL5 and one grain of sample SGM5. They all display the same W-shaped pattern. No significant zoning in major elements is observed in the garnet. (See text for discussion.) (b–d) Chondrite-normalized REE pattern of garnet from three samples.

rare inclusions of monazite. The largest garnet blasts are observed in sample SGL5, where they include monazite and xenotime in the intermediate zone (xenotime in this zone is mainly found as part of composite inclusions) and in the rim (Fig. 5c and d). Zircon is a common inclusion throughout the garnet in all samples investigated.

Garnet chondrite-normalized REE patterns for the three samples show similar features (Fig. 10c–e) that are common to high-grade garnet in granulites and migmatites (Degeling *et al.*, 2001; Hermann & Rubatto, 2003; Whitehouse & Platt, 2003; Kelly & Harley, 2005): LREE depletion well below chondrite values (La mainly 0·15–0·02), strong negative Eu anomaly (Eu/Eu* 0·014–0·028) and relative HREE enrichment. A significant variation is observed between SGP3 garnet and the higher grade ones: in SGP3 HREE enrichment is limited (Lu/Gd 0·4–12, mostly 1–4) and some of the patterns for the intermediate zone are virtually flat in the HREE (Lu/Gd 0·44–1·8). HREE enrichment is maximum in sample SGL5, where Lu/Gd for the garnet core and rim is 25–43. Regardless of the amount of relative HREE enrichment, in each sample the garnet core has a more enriched pattern than the intermediate zone. Despite differences in the HREE, the negative Eu anomaly and LREE are remarkably similar across domains or grains, with the single exception of some higher LREE content in the SGP3 garnet.

DISCUSSION

Age interpretation

Two major types of zircon crystal were found in the samples dated: (1) pre ~1800 Ma domains, which appear as rounded grains at low grade or as zircon cores at higher grade; (2) CL-dark, poorly zoned, euhedral overgrowths dated at around 1800 Ma, which overgrow cores in the high-grade samples SGL3, SGL5, SGM5 and SGRA. Monazite separated from seven samples, including the granite, has a similar age pattern to zircon, but with a larger 1800 Ma component already present at lower grade. A range of ages can be defined in this extensive dataset and their interpretation is presented below.

Metamorphic age

The major age component found in monazite (monazite rims at low grade and entire monazite grains at high grade) is in the range 1790 ± 7 to 1806 ± 6 Ma (Fig. 11). This age is interpreted as dating metamorphism, in agreement with the zircon data. Additionally, monazite has been found as inclusions in the intermediate part and the rim of the garnet in the high-grade samples (Fig. 5). In these granulites, garnet formed during high-grade metamorphism.

The second zircon type, which occurs in SGP3, the high-grade migmatites (SGL5–SGM5) and the granite,

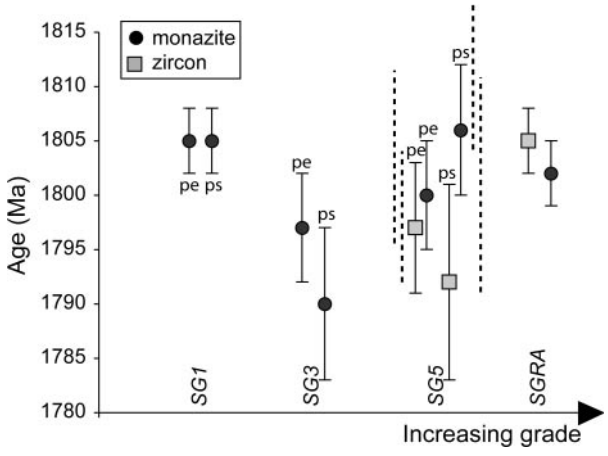

Fig. 11. Monazite and zircon ages vs increasing metamorphic grade. Error bars represent 95% confidence level. For monazite in sample SGM5 and SGL5 the average monazite age, and those of cores and rims (dashed lines) are plotted. Pe, metapelite; ps, metapsammite. (See text for discussion.)

has the same age as most of the monazite (Fig. 11). The characteristics of this zircon type (poor zoning, rims surrounding inherited cores, low Th/U $\leq$0·1) are typical of high-grade metamorphic zircon as found in migmatites (e.g. Williams & Claesson, 1987; Williams *et al.*, 1996; Oliver *et al.*, 1999; Rubatto *et al.*, 2001; Corfu *et al.*, 2003). This zircon type is thus interpreted in a general sense as dating the anatectic event and high-grade metamorphism at Mount Stafford. A more rigorous correlation between age and metamorphism is discussed in the following sections.

The range of monazite ages between samples (particularly between SGP3 and the rest of the samples) is larger than can be explained by analytical error. This range and the possibility of age differences between monazite cores and rims deserve consideration. The youngest monazite age was obtained from metapelite SGP3 (1790 ± 7 Ma) and is significantly lower than ages of four of the other monazite samples at higher and lower grade. The analytical session during which monazite from SGP3 and SGL3 was dated featured a significant amount of excess ^{204}Pb, despite the use of energy filtering to reduce molecular interferences (see Rubatto *et al.*, 2001). If ^{204}Pb is overestimated, the calculated ages will be overcorrected and thus younger than the real age. During data evaluation, the analyses were corrected for ^{204}Pb over-counts using the standard. However, it is still possible that the low apparent age of sample SGP3 is an analytical artefact. Therefore, the age of this sample should be treated with caution and we do not place any geological significance on the age difference.

The apparent difference in age between core and rim in monazite from the two highest-grade granulites (sample SGL5 and SGM5) cannot be discarded as an analytical artefact. Data from both samples were collected in the same analytical session, during which cores and rims were analysed alternately. The BSE imaging shows a marked change in zoning between monazite cores and rims, and in sample SGM5 the chemical composition (particularly Th and U contents, Th/U and Eu anomaly, Fig. 7 and Electronic Appendix 2, http://www.petrology.oxfordjournals.org) of cores and rims is distinguishable. A similar compositional difference is present in monazite cores and rims of sample SGL3, although no age difference could be detected or resolved in that case. There is thus an indication that the physical and chemical conditions changed in the course of monazite growth. Although the analytical uncertainties of the ages (core vs rim in each sample, Fig. 11) overlap, the zoning and chemical differences support a two-stage growth for the monazite within a time span of <10 Myr. Multiple monazite growth–recrystallization episodes within a single metamorphic event have been documented in several cases following intra-crystalline age variation and Y zoning (e.g. Fitzsimons *et al.*, 1997; Foster *et al.*, 2002; Hermann & Rubatto, 2003). The possible scenarios for two episodes of monazite growth are discussed below.

Magmatic age

The metamorphic rocks and the granite yielded indistinguishable zircon and monazite ages (Fig. 11). The characteristics (zoning and chemical composition) of these minerals in both rock types are similar. The age of the zircon rims and the monazite from the granite are interpreted as dating the granite crystallization. However, the distinction between high-grade metamorphism and anatectic magmatism is semantic, as both probably occurred simultaneously in the same geological setting. The identical age of granite emplacement and high-grade metamorphism confirms the complex field relationships between granite and granulites described earlier and the hypothesis that magmatism and metamorphism at Mount Stafford are interrelated (Vernon *et al.*, 1990; Collins & Vernon, 1991). It also implies that it is unlikely that the granite was the heat source for the high-temperature metamorphism, and that another heat source has to be found.

A previous ion-microprobe study of zircon from the Mount Stafford granite determined an age of 1818 ± 15 Ma for the formation of the most external zircon overgrowth, and was taken as dating the granite crystallization (Collins & Williams, 1995). This age is within analytical error of our age (1805 ± 3 Ma). The larger analytical spread of the Collins & Williams age is partly attributed to reverse discordant analyses and possibly mixing with older (e.g. ~1857 Ma) components found in that zircon population (the analyses were

performed without prior CL imaging). The monazite from the granite does not show the complexity of the zircon and its age of 1802 ± 3 Ma is in agreement with the zircon rim age and the best estimate of the granite crystallization. This age estimate indicates that the Mount Stafford granite is coeval with the Yaningidjara Orthogneiss in the adjacent Reynolds Range (SE of Mount Stafford), which has been dated by U–Pb on zircon at 1806 ± 6 Ma (Vry *et al.*, 1996).

Detrital and inherited ages

The pre-1800 Ma zircon is interpreted as detrital because of its rounded aspect, abraded surface (in the low-grade samples), variable zoning pattern, and age. The majority of these domains have oscillatory zoning and Th/U composition >0·1, which suggest an igneous origin (e.g. Williams & Claesson, 1987; Heaman *et al.*, 1990). Some of the pre-1800 Ma domains, however, have features more typical of metamorphic domains with low Th/U values, weak or no zoning, and inclusions of biotite and cordierite (1820 and 1860 Ma domains, Fig. 4). These domains could have been formed during high-grade metamorphism or partial melting in some of the rocks from which the detrital zircon grains originated. The youngest concordant age measured on the likely metamorphic detrital grains is 1823 ± 5 Ma (eight analyses from samples SGP3 and SGL3 mainly on dark zircon rims, MSWD 0·5, 95% c.l.). Similarly, the youngest high Th/U domain with weak oscillatory zoning yielded a concordant age of ~1820 Ma (two analyses on the same domain, SGP3-9.1 and 9.2). Another six analyses on metamorphic-looking zircon rims from the same samples yielded slightly older ages averaging at 1842 ± 3 Ma (MSWD 0·85). Samples SGP1 and SGP3 contain a population of six zircon rims averaging at 1856 ± 3 Ma (MSWD 0·41), which is also the age of a concordant zircon core with undoubtedly detrital features (1854 ± 11 Ma). Another six analyses cluster at 1871 ± 4 Ma (MSWD 0·17). From this dataset, we conclude that there is sufficient evidence to suggest deposition of the Mount Stafford Beds at or before ~1820 Ma. The deposition of the Lander Rock Beds, to which the Mount Stafford Beds are correlated, has been inferred to be younger than 1838 Ma, the age of the youngest detrital zircon core found in the Lander metasediments (Vry *et al.*, 1996). Similarly, ion microprobe work on the low-grade Mount Stafford Beds indicates deposition after about 1840 Ma (Claoué-Long, 2003). Our work, although limited in the number of detrital grains analysed, points to a younger depositional age of the Mount Stafford Beds, closer to the age of metamorphism. Additionally, this work confirms the existence of a significant ~1840–1870 Ma geological event in the source region of the Mount Stafford Beds. In the geology of the Arunta Inlier, the main event predating the Stafford metamorphism has generally been identified as the 1850–1880 Ma Barramundi Orogeny, which affected the northern Arunta Inlier and the Australian continent (Page, 1988). A number of detrital zircons found in the samples investigated can thus be related to this regional event.

Monazite in the low-grade samples (SGP1 and SGP3) that show a low degree of partial melting appears to have a particular patchy zoning pattern that is rarely observed at higher grade (Fig. 2). Commonly, but not always, these domains preserve a $^{207}Pb/^{206}Pb$ age significantly older than 1800 Ma (up to ~2450 Ma). Such inherited Pb components are absent in samples at higher grade or that experienced a higher degree of melting, despite the presence of core–rim structures (see below). This is consistent with the progressive loss of inherited Pb from the monazite with increasing metamorphic grade and degree of partial melting. The cause of progressive disappearance of inherited monazite could potentially be either diffusive loss of radiogenic Pb or complete dissolution of pre-existing monazite during melting. If recent estimates of the closure temperature for Pb diffusion in monazite (>900°C Montel *et al.*, 2000; Cherniak *et al.*, 2004) are correct, then Pb diffusion was not possible at Mount Stafford and dissolution of inherited monazite is more likely. The limited number of old monazites analysed (11) makes it impossible to establish the geological significance of any of the pre-1800 Ma ages found in the monazite cores.

Zircon and monazite behaviour during metamorphism

The detailed geochronological work allows determination of which domains in zircon and monazite formed during prograde metamorphism. Trace element compositions, determined on the same domains, help to link the growth of the accessory phases to the main mineral assemblage. In this section we link this information to the detailed phase petrology study of White *et al.* (2003), to constrain the response of zircon and monazite to partial melting processes. Figure 12 shows our sample localities compared with calculated melt production in a representative metapelite and metapsammite composition (White *et al.*, 2003) appropriate for our sample suite.

In a number of previous studies, it has been observed that during prograde metamorphism of metapelites the first occurrence of significant zircon overgrowths generally coincides with partial melting (e.g. Vavra *et al.*, 1996; Rubatto *et al.*, 2001; Williams, 2001). Overgrowths then progressively increase in volume with increase in temperature and degree of melting, the latter being partly controlled by the whole-rock composition

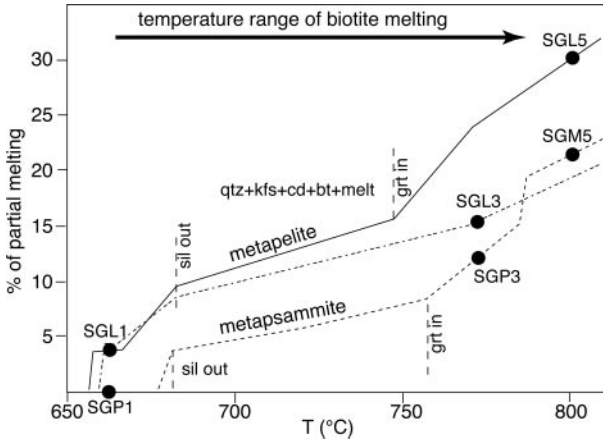

Fig. 12. Calculated melt production in a metapelite and metapsammite composition [according to White *et al.* (2003)] appropriate for our sample suite. The samples investigated in this work are reported on the lines indicating comparable compositions.

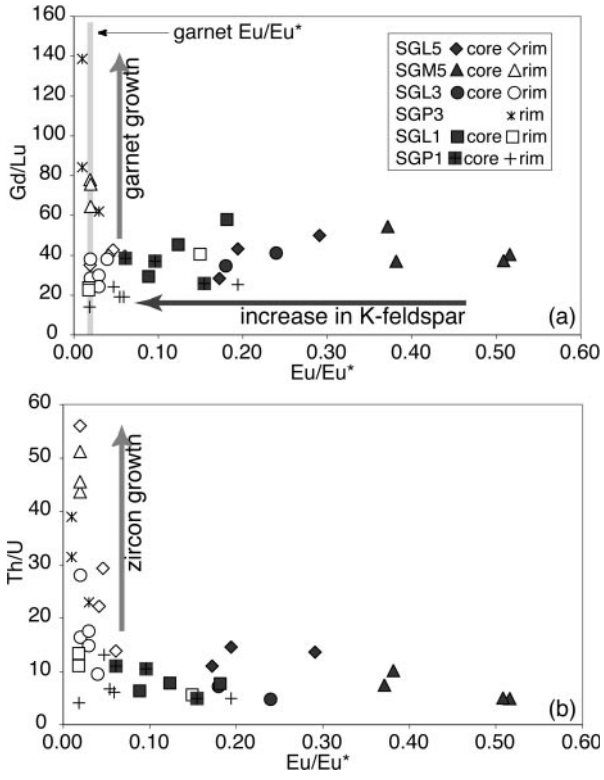

Fig. 13. Monazite chemical variation. (a) Eu anomaly (Eu/Eu*) vs Gd/Lu; for each sample, monazite cores have lower Gd/Lu and a weaker negative Eu anomaly than corresponding rims. The effects of increasing K-feldspar crystallization and garnet growth are indicated with arrows. The value of Eu/Eu* in garnet is reported for comparison. (b) Eu anomaly vs Th/U: monazite rims have higher Th/U than cores in all samples where metamorphic zircon overgrowths were observed. [For legend see (a).] A difference in age between monazite cores and rims was detected in sample SGL5 and particularly in sample SGM5, where the chemical distinction is more prominent. Core–rim definition is based on BSE imaging. Analyses that represent a mix of core and rim are not plotted.

(pelites vs psammites) (Vavra *et al.*, 1996; Rubatto *et al.*, 2001). In the Mount Stafford sequence, however, metamorphic zircon of sufficient size to be detected by CL imaging is absent from samples in the lower part of the sequence, which experienced a low degree of partial melting (e.g. SGL1). The first appearance of metamorphic zircon overgrowths occurs in metapelite SGL3, which was metamorphosed to temperatures well in excess of the wet pelite solidus. This example demonstrates that melt alone is not a sufficient criterion to produce zircon overgrowth and that temperature and bulk-rock composition also play an important role.

The formation of metamorphic monazite in the prograde sequence at Mount Stafford precedes that of metamorphic zircon overgrowths: in the lower-grade samples (localities SG1 and SG3) metamorphic monazite is found, whereas no or only rare (SGL3) ~1800 Ma zircon overgrowths occur. Monazite formation occurs in Zone 2 at temperatures around 650°C, and it is possible that metamorphic monazite first appeared in the sequence at even lower grade. On the other hand, the first traces of metamorphic zircon overgrowths are observed only in Zone 3 (sample SGL3) at temperatures at least 125°C higher than the appearance of monazite. This confirms previous reports that monazite is generally more sensitive than zircon to medium-grade metamorphism (e.g. Smith & Barreiro, 1990; Kingsbury *et al.*, 1993; Rubatto *et al.*, 2001).

Monazite preserves more differences between metapelites and metapsammites than does zircon. Monazite from metapsammite SGP3 still contains a significant volume of inherited cores older than 1800 Ma. In the adjacent metapelite SGL3, a core–rim structure is present, marked by differences in zoning and composition, but no inherited Pb was found in the cores. In the higher-grade samples, monazite has a core–rim structure marked by chemical differences and a subtle age difference. The main chemical difference is that core compositions have generally a much less pronounced negative Eu anomaly than rims (Fig. 13a). In addition, monazite rims in the higher-grade rocks have a steeper REE pattern, resulting in higher Gd/Lu (Fig. 13a) than metamorphic cores or samples at lower grade. To explain these features the principle sub-solidus and melting reactions occurring in the Mount Stafford sequence (e.g. White *et al.*, 2003) have to be considered. Because of the low-pressure environment, muscovite breaks down in sub-solidus conditions [mineral abbreviations Liq = liquid and according to Bucher & Frey (1994)]:

$$\mathrm{Ms} + \mathrm{Qtz} \rightarrow \mathrm{Kfs} + \mathrm{Sil} + \mathrm{H_2O}. \qquad (1)$$

The appearance of melt is related to the continuous breakdown of biotite with increasing temperature during

the following reactions:

$$\mathrm{Bt} + \mathrm{Sil} + \mathrm{Qtz} \rightarrow \mathrm{Crd} + \mathrm{Kfs} + \mathrm{Liq} \quad (2)$$

$$\mathrm{Bt} + \mathrm{Sil} \rightarrow \mathrm{Crd} + \mathrm{Spl} + \mathrm{Kfs} + \mathrm{Liq} \quad (3)$$

$$\mathrm{Bt} + \mathrm{Crd} + \mathrm{Qtz} \rightarrow \mathrm{Grt} + \mathrm{Kfs} + \mathrm{Liq} \quad (4)$$

$$\mathrm{Bt} + \mathrm{Grt} + \mathrm{Qtz} \rightarrow \mathrm{Opx} + \mathrm{Crd} + \mathrm{Kfs} + \mathrm{Liq}. \quad (5)$$

One common feature of all these reactions is the formation of residual K-feldspar. The K-feldspar REE pattern is characterized by a strong positive Eu anomaly (Bea *et al.*, 1994). The present samples, as is common for metapelites and metapsammites at Mount Stafford, contain very little plagioclase (Greenfield *et al.*, 1996). Thus, in the absence of other minerals that might fractionate Eu strongly, the increasing negative Eu anomaly in monazite from core to rim can be explained by prograde monazite growth with coexisting K-feldspar. Even sample SGP1, which shows no evidence of melting, displays such a trend in Eu anomaly. Consequently, we suggest that in this sample monazite rim formation was related to the sub-solidus reaction (1) that is dated at 1805 ± 3 Ma. During initial partial melting, in addition to K-feldspar, cordierite and spinel are formed. These minerals do not incorporate significant amounts of REE and hence the only feature changing is the increasing negative Eu anomaly for monazite that forms related to melting reactions (2) and (3). This is supported by the observation that the decreasing Eu anomaly is the only distinct REE feature in monazite in samples with the assemblage Qtz + Crd + Bt + Kfs + Spl (SGL1, SGP1, SGL3). Because garnet preferentially incorporates HREE with respect to MREE (Fig. 10) the appearance of garnet according to melting reaction (4) influences the REE pattern of coexisting minerals. In fact, the composition of the monazite rim in the three samples containing garnet (SGP3, SGM5, SGL5) displays an increase in Gd/Lu (Fig. 13a). This increase is most pronounced in the metapsammite samples that contain abundant garnet. Interestingly,the Eu anomaly in garnet is similarly high as in these monazite rims (Fig. 13a), further supporting the hypothesis that the metamorphic cores of monazite in the high-grade samples formed prior to garnet growth. This is most visible in sample SGM5. Combined with the ages of this sample we suggest that these cores formed during reactions (1)–(3) at 1811 ± 7 Ma and the rim formed related to reaction (4) at 1801 ± 10 Ma. This relation of monazite age to metamorphic reaction shows that the heating rate is beyond the resolution of the monazite dating.

The variation in Th/U compared with the increasing negative Eu anomaly is another interesting feature in monazite (Fig. 13b). The Th/U ratio remains nearly constant in the metamorphic monazite cores and also in the rims of the lowest-grade sample. This indicates that no phase that strongly partitions Th and/or U formed contemporaneously. In contrast, the monazite rim compositions of the higher-grade samples display a strong increase in Th/U. This increase coincides with the appearance of U-rich metamorphic zircon rims with low Th/U. This correlation suggests that coexisting zircon and monazite strongly affect their respective Th/U.

The respective trace element compositions of zircon and monazite are similar in both the metapelites and the metapsammites. The patterns shown in Fig. 7 for the pairs SGP3–SGL3 and SGM5–SGL5 show only small differences: zircon in the samples that display stronger evidence of melting is slightly more enriched in HREE than in the metapsammites where melt was less abundant (Lu/Gd of 58–70 and 24–64, respectively); monazite is more strongly depleted in HREE in SGP3 and SGM5 with respect to the corresponding pelitic layers (SGL3 and SGL5, Fig. 8). In absolute terms, both minerals in metapelites that underwent significant melting are marginally richer in HREE than in the corresponding metapsammite where melting was relatively less. A similar HREE enrichment in the accessory minerals was reported for leucosomes in granulites of the nearby Reynolds Range (Rubatto *et al.*, 2001).

The similarity of accessory mineral compositions between metapelites and metapsammites layers suggests that the accessory minerals in both rocks types formed via similar processes in rocks that have similar to identical assemblages. In fact, the main difference between metapelites and metapsammites is the amount of quartz, which will not affect the REE budget.

Garnet zoning

Whereas the major element compositions of garnet show very little variation between and within samples (Electronic Appendix 3, http://www.petrology.oxfordjournals.org), garnet is zoned in its trace element content. This decoupling is due to the faster diffusion of major divalent elements, with respect to trace elements, particularly trivalent REE and quadrivalent high field strength elements (HFSE) (Chernoff & Carlson, 1999; Otamendi *et al.*, 2002; Van Orman *et al.*, 2002). The different behaviour of trace and major elements has been documented in amphibolite- to granulite-facies garnet (e.g. Pyle & Spear, 1999; Yang & Rivers, 2002; Hermann & Rubatto, 2003; Buick *et al.*, 2006).

At the low pressures of metamorphism, and for the bulk compositions of the Mount Stafford metapelites and metapsammites, no garnet is expected to grow along the sub-solidus *P–T* path (White *et al.*, 2003). Therefore, all

garnet growth in the studied rocks is due to reaction (4). Calculated pseudosections (White *et al.*, 2003) indicate that garnet growth started in the metapsammites and metapelites with suitable compositions at about 750°C (Fig. 13). The trace element zoning in the garnet can be subdivided into two major sections: a central bell-shape with trace element depleted flanks (a gradual transition from core to intermediate zone) followed by a HREE and Y enrichment zone at the rim. The bell-shaped growth profile, with a progressive decrease of trace element concentrations from core to rim, is commonly observed in high-grade garnet in the presence of melt (Pyle & Spear, 1999; Otamendi *et al.*, 2002; Hermann & Rubatto, 2003; Whitehouse & Platt, 2003). This feature is interpreted as reflecting Rayleigh distillation during prograde garnet growth in the presence of melt (Pyle & Spear, 1999; Otamendi *et al.*, 2002). Xenotime or monazite inclusions were not found in the garnet core, suggesting that Y and REE were not buffered during this initial growth stage. Not surprisingly, the garnet core is poor in P compared with the intermediate zone, where monazite and xenotime are found.

The second zone (i.e. the narrow rim enriched in compatible elements) is likely to reflect resorption of garnet in contact with melt during a decrease in temperature and pressure. In a closed system without significant melt loss, as is the case for Mount Stafford granulites, garnet should retrogress by back-reaction with the crystallizing melt (White *et al.*, 2003). The formation of a trace element enriched zone by melt resorption has been previously suggested by Otamendi *et al.* (2002) and studied by Storkey *et al.* (2005), who investigated garnet from a partially molten metabasite. However, in previous reports, garnet resorption is accompanied by Mn enrichment at the rims, which is not observed in the Mount Stafford garnets (CaO and MnO remain constant from core to rim). According to the pseudosections calculated by White *et al.* (2003) for garnet-bearing metapelites or metapsammites (e.g. their fig. 6 and fig. 11, respectively), the molar mode contours for garnet change slope from the biotite-bearing to the biotite-out field with increasing temperature. A rock with a prograde path with moderate increase in pressure (White *et al.*, 2003) would first form garnet at the expense of biotite (up to ~760°C at 3·5 kbar), then, once it enters the biotite-free field (>760°C), it would virtually stop growing garnet. During the early part of cooling, around 750–800°C, biotite would form by back-reaction with the melt. The presence of melt has been widely documented in the Mount Stafford granulites (Greenfield *et al.*, 1996; White *et al.*, 2003) and formation of secondary biotite at garnet rims is common. If garnet resorption occurred at such high temperatures (750–800°C), it is to be expected that a Mn-rich rim would not be preserved because of fast Mn diffusion. Xenotime is present as rare inclusions in the high-Y rim (Fig. 5e), indicating that xenotime also formed during back-reaction.

A Y-rich annulus has been observed via element mapping in one garnet from SGL5. This annulus appears in only one of the three garnets mapped and is thus probably a local phenomenon. A number of mechanisms have been proposed for the growth of Y-rich annular rings in garnet, such as fluid infiltration, changes in garnet growth rates, breakdown of Y-enriched phases, and garnet resorption and renewed growth [see Pyle & Spear (1999) for a review]. The most likely explanation for the formation of the annulus in some Mount Stafford granulites is local garnet resorption and renewed growth, as extensively documented by Pyle & Spear (1999). A limited period of garnet resorption close to peak metamorphic conditions could be related to melting reaction (5), which locally consumes garnet, and some garnet regrowth could have occurred during initial high-temperature cooling.

Trace elements to link monazite and zircon to garnet growth

U–Pb ages of monazite and zircon in high-grade rocks are most commonly interpreted as dating the metamorphic peak. In reality, detailed studies that combined geochronology with other observations (inclusions, trace elements or reactions) have often found that zircon and monazite formation occur at the metamorphic peak and during decompression or cooling (Vavra *et al.*, 1996; Williams *et al.*, 1996; Degeling *et al.*, 2001; Hermann *et al.*, 2001; Hermann & Rubatto, 2003): cooling induces melt crystallization, which in turn induces zircon and monazite crystallization (Roberts & Finger, 1997).

At Mount Stafford, garnet, zircon and most of the monazite grew in the presence of melt. Such a situation is ideal to study the trace element partitioning between these phases. This potentially permits the growth of zircon and monazite to be related to that of garnet, and hence to metamorphic conditions (Rubatto, 2002; Hermann & Rubatto, 2003; Whitehouse & Platt, 2003; Hokada & Harley, 2004).

Garnet is contained in three of the samples dated: SGP3, SGM5 and SGL5. The garnet zoning is better documented in the higher-grade samples, SGM5 and SGL5, for which both monazite and zircon data are available. Thus, we present partitioning data only for these two samples. Inclusions of monazite and zircon are found in the intermediate part of the garnet and in the garnet rim. Whereas monazite inclusions are necessarily metamorphic (no inherited monazite was found in these high-grade samples), zircon inclusions could be inherited (zircon inclusions in garnet are <50 μm and CL images of such inclusions are not indicative of either metamorphic rims or inherited cores).

The garnet REE content in the two samples varies between the high-REE core, the low-REE garnet in the intermediate zone, and the narrow and high-REE garnet rim. Monazite/garnet and zircon/garnet distribution coefficients ($D_{Mnz/Grt}$ and $D_{Zrn/Grt}$, respectively) for trace elements were calculated using the average composition of the garnet intermediate zone and representative core and rim analyses. For the accessory phases, an average metamorphic zircon and average monazite rim (which have been shown to coexist with garnet; Fig. 13a) composition was used. Partitioning for the LREE might be subject to large errors and scatter, as a result of the low concentration and thus difficulty in measuring these elements in garnet and zircon. Th and U concentrations in zircon and monazite can vary significantly within a single crystal, particularly in zircon; the distribution coefficients for Th and U are thus subject to larger variations and the values reported represent an average. Values for Y and the MREE–HREE are the most robust and indicative, and are thus plotted in Fig. 14.

For both samples, partitioning between the ~1800 Ma zircon and the low-REE garnet intermediate zone is similar, with $D_{Zrn/Grt}$ for HREE increasing with atomic number from 0·75 for Gd to ~7 for Lu. Partitioning between zircon and the high-REE garnet core and resorption rim is significantly lower (Lu 0·9–1·5), with a flat pattern for the HREE. The values for the intermediate garnet zone agree with partitioning in rocks that underwent similar metamorphic conditions: a granulite in the nearby Reynolds Range (750–800°C and 4·5–5 kbar, Rubatto, 2002), a restitic granulite from the Alps (800–850°C and 10 kbar, Hermann & Rubatto, 2003) and a granulitic gneiss from the Limpopo Belt (>800°C and 8–10 kbar, Buick *et al.*, 2006). The $D_{Zrn/Grt}$ values calculated for the high-REE garnet are closer to the values reported by other studies (Whitehouse & Platt, 2003; Hokada & Harley, 2004; Kelly & Harley, 2005). The Antarctic rocks investigated by Hokada & Harley (2004) and Kelly & Harley (2005) underwent extreme metamorphic conditions with temperatures reaching 1100°C. For none of the samples they investigated do good textural relationships exist between garnet and zircon. Element diffusion at high temperatures, higher metamorphic conditions and much more grossular-rich garnet composition [$alm_{0·52}prp_{0·46}grs_{0·024}sps_{0·003}$ in the study by Hokada & Harley (2004)] could also have affected $D_{Zrn/Grt}$. For these reasons we consider the data from the Antarctic rocks (Hokada & Harley, 2004; Kelly & Harley, 2005) an improper comparison for our partitioning. The $D_{Zrn/Grt}$ values reported by Whitehouse & Platt (2003) are from a granulite where garnet formed at conditions of 750–800°C and 8·5–9 kbar and in which metamorphic zircon is included in garnet. Why this dataset disagrees with those obtained from other similar granulite-facies rocks (Rubatto, 2002; Hermann & Rubatto, 2003; Buick *et al.*, 2006) is unclear.

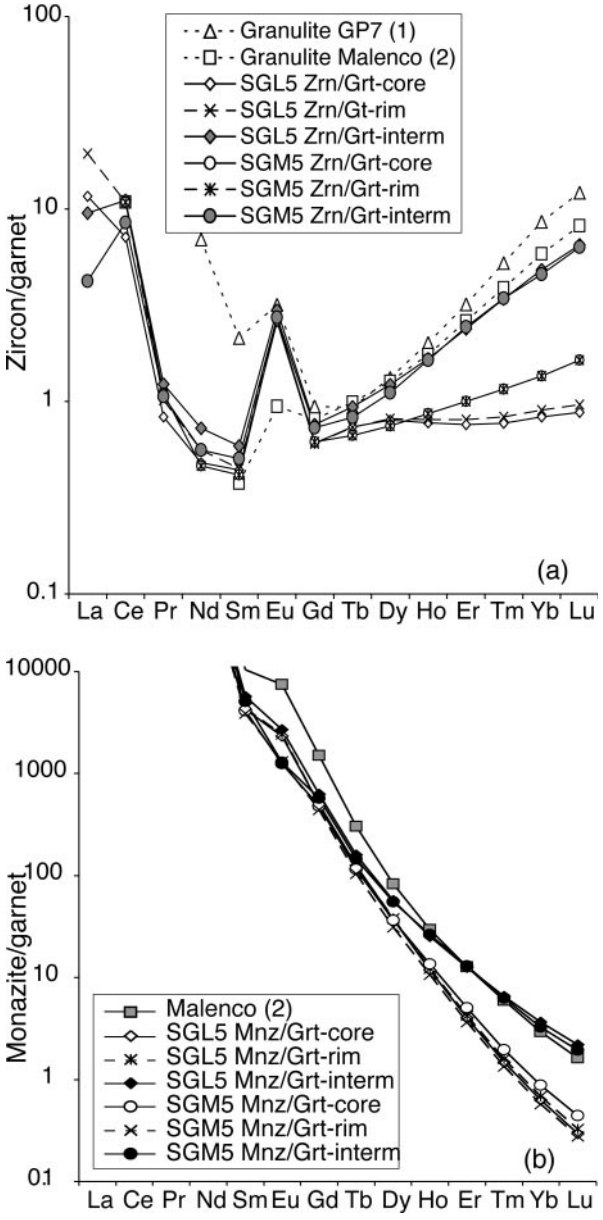

Fig. 14. Calculated distribution coefficients of REE between zircon and garnet (a) and monazite and garnet (b) for the two samples SGL5 and SGM5. Partitioning is calculated between the ~1800 Ma zircon or monazite rim and different garnet compositions (core, intermediate or rim) in the same sample. For comparison, data from (1) Rubatto (2003) and (2) Hermann & Rubatto (2003) are plotted.

For monazite, the partitioning is again similar in both samples. Distribution coefficients strongly decrease across the REE; if the low-REE garnet of the intermediate zone is taken, the $D_{Mnz/Grt}$ for HREE is higher (Gd to Lu ~600–2) than that obtained for the

Table 2: Distribution coefficients between zircon, monazite and garnet

	Zrn/Grt SGM5	Zrn/Grt SGL5	Mnz/Grt SGM5	Mnz/Grt SGL5	Mnz/Grt SGL5	Mnz/Zrn SGL5	Mnz/Zrn SGM5
P	6·5	6·8	n.a.	n.a.	n.a.	n.a.	n.a.
Ca	n.a.	n.a.	0·93	0·90	1·01	n.a.	n.a.
Ti	n.a.	n.a.	0·053	0·058	0·058	n.a.	n.a.
Y	2·0	1·9	23	21	22	11	12
Zr	n.a.	n.a.	0·17	0·18	0·18	n.a.	n.a.
Nb	90	101	14	25	24	0·24	0·15
La	3·6	9·5	7356737	12172786	1230000	1280000	2050000
Ce	8·1	11·1	2385332	3207594	321000	289000	295000
Pr	1·0	1·2	460342	567768	566000	461000	551000
Nd	0·6	0·7	103710	112660	113000	156000	184000
Sm	0·5	0·6	5095	5936	5690	10100	10000
Eu	2·8	3·0	1283	7742	2690	2590	466
Gd	0·73	0·76	571	644	629	848	779
Tb	0·84	0·94	146	163	159	174	174
Dy	1·1	1·2	55	56	57	46	49
Ho	1·7	1·7	26	24	25	15	16
Er	2·6	2·4	13	12	13	5·1	5·0
Tm	3·7	3·4	6·3	6·5	6·5	1·9	1·7
Yb	5·0	4·8	3·2	3·8	3·7	0·78	0·65
Lu	7·2	6·5	1·9	2·3	2·2	0·35	0·27
Hf	27800	20300	0·14	0·15	0·18	n.a.	n.a.
Ta	n.a.	n.a.	1·34	0·32	0·31	n.a.	n.a.
Th	4580	3810	6960000	4470000	5360000	1170	1520
U	28600	42000	58700	190000	193000	4·5	2·1

n.a., not analysed.

high-REE garnet in the core and rim (Gd to Lu ~500–0·4). The value for the low-REE garnet is in agreement with previously published data (Hermann & Rubatto, 2003; Buick *et al.*, 2006). The equilibrium is supported by the observation that inclusions of monazite in the high-grade samples, in which no inherited monazite is preserved, occur in the intermediate garnet zone, but not in the high-REE garnet cores.

In summary, $D_{Zrn/Grt}$ and $D_{Mnz/Grt}$ calculated with respect to the composition of the intermediate zone of the garnet agree with most of the published data for granulites that underwent similar metamorphic conditions to Mount Stafford. This suggests that the zircon and monazite formed in equilibrium with the low-REE intermediate garnet zone. This zone in the garnet is interpreted as having formed shortly before the metamorphic peak. The calculated partitioning provides supporting evidence that zircon and monazite at Mount Stafford formed close to the metamorphic peak.

Zircon and monazite rims in samples SGL5 and SGM5 both show equilibrium partitioning with the same garnet zone, and have similar ages. It follows that they formed at the same time in the metamorphic history and thus should be in chemical equilibrium. The trace element partitioning between monazite rims and 1800 Ma zircon rims within the same sample should therefore reflect equilibrium. The values obtained for the two high-grade samples SGL5 and SGM5 are in fact similar to each other (Table 2), with values of Y 11–13, Sm ~10 000, Dy 46–52, Er 5·1–5·5 and Lu 0·35–0·29. These values are remarkably similar to those previously published for coexisting monazite and zircon in other granulites (Hermann & Rubatto, 2003; Buick *et al.*, 2006).

CONCLUSIONS

At Mount Stafford prograde metamorphism from amphibolite to granulite facies and anatexis occurred in the period between 1795 and 1805 Ma, as recorded by zircon and monazite. The emplacement of the Mount Stafford granite, best dated by monazite at 1802 ± 3 Ma,

was synchronous with the high-grade metamorphism. The protoliths to the Mount Stafford metasedimentary sequence were deposited at or after 1820 Ma, as suggested by the youngest detrital zircon found in this study.

During the ~1800 Ma high-temperature event, metamorphic zircon formation did not coincide with the first appearance of melt. Significant zircon overgrowths appeared only at higher temperature in metapelitic layers, and their formation was delayed in the metapsammites, probably because of the relatively lower degree of melting. Metamorphic monazite, on the other hand, was present in both metapelites and metapsammites at or before melting occurred. The detailed study of the trace element composition of metamorphic monazite showed that monazite grew over an extended temperature interval from sub-solidus to peak metamorphic conditions. In some monazite grains there is clear evidence for two distinct monazite growth periods, one before and one concomitant with garnet growth. However, ages obtained from these different domains are not distinguishable within error (<20 Ma). During prograde metamorphism, monazite progressively lost its inherited Pb components, probably by dissolution in the melt of any detrital grain, whereas zircon inheritance is abundant up to peak conditions (~800°C and 3·3–4·0 kbar).

In the highest-grade granulites, garnet formation is widespread and occurred during prograde metamorphism, particularly by biotite melting reactions (garnet core to intermediate zone). Garnet resorption (garnet rim) occurred in the initial stage of cooling, promoted by the fact that melt segregation was limited. The trace element partitioning between zircon and garnet, and monazite and garnet indicates that these U-rich accessory minerals formed in equilibrium with the intermediate part of the garnet, i.e. at the end of the prograde path, close to the metamorphic peak.

ACKNOWLEDGEMENTS

We thank Ian Williams for constructive discussion at different stages of this project. The reviews by Julia Baldwin and Richard White helped to improve the manuscript. The Electron Microscopy Unit at the Australian National University is thanked for access to the SEM facilities. This work was financially supported by the ARC and the Swiss National Science Foundation. D.R. acknowledges an ARC Queen Elisabeth II Fellowship and I.S.B. an ARC Australian Professorial Fellowship.

SUPPLEMENTARY DATA

Supplementary data for this paper are available at *Journal of Petrology* online.

REFERENCES

Bea, F., Pereira, M. D. & Stroh, A. (1994). Mineral/leucosome trace-element partitioning in a peraluminous migmatite (a laser ablation-ICP-MS study). *Chemical Geology* **117**, 291–312.

Blake, D. H. & Page, R. W. (1988). The Proterozoic Davenport province, central Australia: regional geology and geochronology. *Precambrian Research* **40/41**, 329–340.

Bucher, K. & Frey, M. (1994). *Petrogenesis of Metamorphic Rocks*. Berlin: Springer.

Buick, I. S., Hermann, J., Williams, I. S., Gibson, R. & Rubatto, D. (2006). A SHRIMP U–Pb and LA-ICP-MS trace element study of the petrogenesis of garnet–cordierite–orthoamphibole gneisses from the Central Zone of the Limpopo Belt, South Africa. *Lithos* **88**, 150–172.

Cesare, B., Marchesi, C., Hermann, J. & Gómez-Pugnaire, M. T. (2003). Primary melt inclusions in andalusite from anatectic graphitic metapelites: iImplications for the position of the Al_2SiO_5 triple point. *Geology* **31**, 573–576.

Cherniak, D. J., Watson, E. B., Grove, M. & Harrison, T. M. (2004). Pb diffusion in monazite: a combined RBS/SIMS study. *Geochimica et Cosmochimica Acta* **68**, 829–840.

Chernoff, C. B. & Carlson, W. D. (1999). Trace element zoning as a record of chemical disequilibrium during garnet growth. *Geology* **27**, 555–558.

Claoué-Long, J. C. (2003). Event chronology in the Arunta region. In: *AGES Conference Abstracts Volume*. Alice Springs: Northern Territory Geological Survey, pp. 23–24.

Clarke, D. B., Dorais, M., Barbarin, B., Barker, D., Cesare, B. & Clarke, G. *et al.* (2005). Occurrence and origin of andalusite in peraluminous felsic igneous rocks. *Journal of Petrology* **46**, 441–472.

Clarke, G. L., Collins, W. J. & Vernon, R. H. (1990). Successive overprinting granulite facies metamorphic events in the Anmatjira Range, central Australia. *Journal of Metamorphic Geology* **8**, 65–88.

Collins, W. J. & Vernon, R. H. (1991). Orogeny associated with anticlockwise *P–T–t* paths: evidence from low-*P*, high-*T* metamorphic terranes in the Arunta Inlier, central Australia. *Geology* **19**, 835–838.

Collins, W. J. & Williams, I. S. (1995). SHRIMP ionprobe dating of short-lived Proterozoic tectonic cycles in the northern Arunta Inlier, central Australia. *Precambrian Research* **71**, 69–89.

Collins, W. J., Vernon, R. H. & Clarke, G. L. (1991). Discrete Proterozoic structural terranes assocaited with low-*P*, high-*T* metamorphism, Anmatjira Range, Arunta Inlier, central Australia: tectonic implications. *Journal of Structural Geology* **13**, 1157–1171.

Compston, W., Williams, I. S. & Meyer, C. (1984). U–Pb geochronology of zircons from lunar breccia 73217 using a sensitive high mass-resolution ion microprobe. *Journal of Geophysical Research* **89**, B525–B534.

Corfu, F., Hanchar, J. M., Hoskin, P. W. O. & Kinny, P. (2003). Atlas of zircon textures. In: Hanchar, J. M. & Hoskin, P. W. O. (eds) *Zircon. Mineralogical Society of America, Reviews in Mineralogy and Geochemistry* **53**, 469–500.

Degeling, H., Eggins, S. & Ellis, D. J. (2001). Zr budget for metamorphic reactions, and the formation of zircon from garnet breakdown. *Journal of Metamorphic Geology* **65**, 749–758.

Eggins, S. M., Rudnick, R. L. & McDonough, W. F. (1998). The composition of peridotites and their minerals: a laser ablation ICP-MS study. *Earth and Planetary Science Letters* **154**, 53–71.

Fitzsimons, I. C. W., Kinny, P. D. & Harley, S. L. (1997). Two stages of zircon and monazite growth in anatectic leucogneiss: SHRIMP constraints on the duration and intensity of Pan-African metamorphism in Prydz Bay, East Antarctica. *Terra Nova* **9**, 47–51.

Fitzsimons, I. C. W., Kinny, P. D., Wetherley, S. & Hollingsworth, D. A. (2005). Bulk chemical control on monazite growth in pelitic schists and implications for U–Pb age data. *Journal of Metamorphic Geology* **23**, 261–277.

Foster, G., Gibson, H. D., Parrish, R. R., Horstwood, M., Fraser, J. & Tindle, A. (2002). Textural, chemical and isotopic insight into the nature and behaviour of metamorphic monazite. *Chemical Geology* **191**, 183–207.

Fraser, G., Ellis, D. & Eggins, S. (1997). Zirconium abundance in granulite-facies minerals, with implications for zircon geochronology in high-grade rocks. *Geology* **25**, 607–610.

Greenfield, J. E., Clarke, G. L., Bland, M. & Clark, D. J. (1996). *In situ* migmatite and hybrid diatexite at Mt. Stafford, central Australia. *Journal of Metamorphic Geology* **14**, 413–426.

Greenfield, J. E., Clarke, G. L. & White, R. W. (1998). A sequence of partial melting reactions at Mt. Stafford, central Australia. *Journal of Metamorphic Geology* **16**, 363–378.

Heaman, L. M., Bowsin, R. & Crocket, J. (1990). The chemical composition of igneous zircon suites: implications for geochemical tracer studies. *Geochimica et Cosmochimica Acta* **54**, 1597–1607.

Hermann, J. & Rubatto, D. (2003). Relating zircon and monazite domains to garnet growth zones: age and duration of granulite facies metamorphism in the Val Malenco lower crust. *Journal of Metamorphic Geology* **21**, 833–852.

Hermann, J., Rubatto, D., Korsakov, A. & Shatsky, V. S. (2001). Multiple zircon growth during fast exhumation of diamondiferous, deeply subducted continental crust (Kokchetav massif, Kazakhstan). *Contributions to Mineralogy and Petrology* **141**, 66–82.

Hinton, R. W. & Upton, B. G. J. (1991). The chemistry of zircon: variations within and between large crystals from syenite and alkali basalt xenoliths. *Geochimica et Cosmochimica Acta* **55**, 3287–3302.

Hokada, T. & Harley, S. L. (2004). Zircon growth in UHT leucosome: constraints from zircon–garnet rare earth elements (REE) relations in Napier Complex, East Antarctica. *Journal of Mineralogical and Petrological Sciences* **99**, 180–190.

Hoskin, P. W. O. & Schaltegger, U. (2003). The composition of zircon and igneous and metamorphic petrogenesis. In: Hanchar, J. M. & Hoskin, P. W. O. (eds.) *Zircon. Mineralogical Society of America, Reviews in Mineralogy and Geochemistry* **53**, 27–62.

Kelly, N. & Harley, S. (2005). An integrated microtextural and chemical approach to zircon geochronology: refining the Archean history of the Napier Complex, east Antarctica. *Contributions to Mineralogy and Petrology* **149**, 57–84.

Kingsbury, J. A., Miller, C. F., Wooden, J. L. & Harrison, M. T. (1993). Monazite paragenesis and U–Pb systematics in rocks of the eastern Mojave Desert, California, U.S.A.: implications for thermochronometry. *Chemical Geology* **110**, 147–167.

Ludwig, K. R. (2000). *Isoplot/Ex Version 2.4. A Geochronological Toolkit for Microsoft Excel, Berkeley Geochronological Centre Special Publication* **1a**.

Montel, J.-M., Kornprobst, J. & Vielzeuf, D. (2000). Preservation of old U–Th–Pb ages in shielded monazite: example from the Beni Boussera Hercynian kinzingites (Marocco). *Journal of Metamorphic Geology* **18**, 335–342.

Oliver, N. H. S., Bodorkos, S., Nemchin, A. A., Kinny, P. D. & Watt, G. R. (1999). Relationships between zircon U–Pb SHRIMP ages and leucosome type in migmatites of the Halls Creek Orogen, Western Australia. *Journal of Petrology* **40**, 1553–1575.

Otamendi, J. E., de la Rosa, J. D., Patiño Douce, A. E. & Castro, A. (2002). Rayleigh fractionation of heavy rare earths and yttrium during metamorphic garnet growth. *Geology* **30**, 159–162.

Paces, J. B. & Miller, J. D. (1993). U–Pb ages of the Duluth complex and related mafic intrusions, northeastern Minnesota: geochronologic insights into physical petrogenetic, paleomagnetic and tectonomagmatic processes associated with the 1·1 Ga mid-continent rift system. *Journal of Geophysical Research* **98**, 13997–14013.

Page, R. W. (1988). Geochronology of early to middle Proterozoic fold belts in northern Australia: a review. *Precambrian Research* **40/41**, 1–19.

Pattison, D. R. M. (1992). Stability of andalusite and sillimanite and the Al_2SiO_5 triple point: constraints from the Ballachulish aureole, Scotland. *Journal of Geology* **100**, 423–446.

Pearce, N. J. G., Perkins, W. T., Westgate, J. A., Gorton, M. P., Jackson, S. E., Neal, C. R. & Chenery, S. P. (1997). A compilation of new and published major and trace element data for NIST SRM 610 and NIST SRM 612 glass reference materials. *Geostandards Newsletter* **21**, 115–144.

Pyle, J. M. & Spear, F. S. (1999). Yttrium zoning in garnet: coupling of major and accessory phases during metamorphic reactions. *Geological Materials Research* **1**, 1–49.

Roberts, M. P. & Finger, F. (1997). Do U–Pb zircon ages from granulites reflect peak metamorphic conditions? *Geology* **25**, 319–322.

Rubatto, D. (2002). Zircon trace element geochemistry: distribution coefficients and the link between U–Pb ages and metamorphism. *Chemical Geology* **184**, 123–138.

Rubatto, D., Williams, I. S. & Buick, I. S. (2001). Zircon and monazite response to prograde metamorphism in the Reynolds Range, central Australia. *Contributions to Mineralogy and Petrology* **140**, 458–468.

Smith, H. A. & Barreiro, B. (1990). Monazite U–Pb dating of staurolite grade metamorphism in pelitic schists. *Contributions to Mineralogy and Petrology* **105**, 602–615.

Storkey, A., Hermann, J., Hand, M. & Buick, I. S. (2005). Using *in situ* trace element determinations to monitor partial melting processes in metabasites. *Journal of Petrology* **46**, 1283–1308.

Sun, S. S. & McDonough, W. F. (1989). Chemical and isotopic systematics of oceanic basalts: implications for mantle composition and processes. In: Sanders, A. D. & Norry, M. J. (eds) *Magmatism in the Ocean Basins. Geological Society, London, Special Publications* **42**, 313–345.

Van Orman, J. A., Grove, T. L., Shimizu, N. & Layne, G. D. (2002). Rare earth element diffusion in a natural pyrope single crystal at 2·8 GPa. *Contributions to Mineralogy and Petrology* **142**, 416–424.

Vavra, G., Gebauer, D., Schmidt, R. & Compston, W. (1996). Multiple zircon growth and recrystallization during polyphase Late Carboniferous to Triassic metamorphism in granulites of the Ivrea Zone (Southern Alps): an ion microprobe (SHRIMP) study. *Contributions to Mineralogy and Petrology* **122**, 337–358.

Vernon, R. H., Clark, D. J. & Collins, W. J. (1990). Local, mid-crustal granulite facies metamorphism and melting, an example in the Mount Stafford area, central Australia. In: Ashworth, J. R. & Brown, M. (eds) *High Temperature Metamorphism and Crustal Anatexis*. London: Unwin & Hyman, pp. 272–315.

Vry, J., Compston, W. & Cartwright, I. (1996). SHRIMP II dating of zircons and monazites: reassessing the timing of high-grade metamorphism and fluid flow in the Reynolds Range, northern Arunta Block, Australia. *Journal of Metamorphic Geology* **14**, 335–350.

Watson, B. E. & Harrison, M. T. (2005). Zircon thermometry reveals minimum melting conditions on earliest Earth. *Science* **308**, 841–844.

White, R. W., Powell, R. & Clarke, G. L. (2003). Prograde metamorphic assemblage evolution during partial melting of metasedimentary rocks at low pressures: migmatites from Mt Stafford, central Australia. *Journal of Petrology* **44**, 1937–1960.

Whitehouse, M. J. & Platt, J. P. (2003). Dating high-grade metamorphism: constraints from rare-earth elements in zircon and garnet. *Contributions to Mineralogy and Petrology* **145**, 61–74.

Williams, I. S. (2001). Response of detrital zircon and monazite, and their U–Pb isotopic systems, to regional metamorphism and host-rock partial melting, Cooma Complex, southeastern Australia. *Australian Journal of Earth Sciences* **48**, 557–580.

Williams, I. S. & Claesson, S. (1987). Isotopic evidence for Precambrian provenance and Caledonian metamorphism of high grade paragneisses from the Seve Nappes, Scandinavian Caledonides. II. Ion microprobe zircon U–Th–Pb. *Contributions to Mineralogy and Petrology* **97**, 205–217.

?Williams, I. S., Buick, I. S. & Cartwright, I. (1996). An extended episode of early Mesoproterozoic metamorphic fluid flow in the Reynolds Range, central Australia. *Journal of Metamorphic Geology* **14**, 29–47.

Wing, B. N., Ferry, J. M. & Harrison, T. M. (2003). Prograde destruction and formation of monazite and allanite during contact and regional metamorphism of pelites: petrology and geochronology. *Contributions to Mineralogy and Petrology* **145**, 228–250.

Yang, P. & Rivers, T. (2002). The origin of Mn and Y annuli in garnet and the thermal dependence of P in garnet and Y in apatite in calc-pelite and pelite, Gagnon terrane, western Labrador. *Geological Materials Research* **4**, 1–35.

Yang, P., Rivers, T. & Jackson, S. (1999). Crystal-chemical and thermal controls on the trace element partitioning between coexisting garnet and biotite in metamorphic rocks from western Labrador. *Canadian Mineralogist* **37**, 443–468.